Genesis of the Mississippi Valley-type Zn-Pb deposit of San Vicente, Central Peru: geologic and isotopic (Sr, O, C, S, Pb) evidences

Fontboté, Lluís; Gorzawski, H.

Economic Geology
Vol. 85, 1990, pp. 1402–1437

Genesis of the Mississippi Valley-Type Zn-Pb Deposit of San Vicente, Central Peru: Geologic and Isotopic (Sr, O, C, S, Pb) Evidence

LLUIS FONTBOTÉ*

Mineralogisch-Petrographisches Institute, Im Neuenheimer Feld 236, D-6900 Heidelberg, Germany

AND HENDRIK GORZAWSKI

Max Planck Institut für Chemie, Postfach 3060, 6500 Mainz, Germany

Abstract

The San Vicente Zn-Pb ore deposit is situated 300 km east of Lima in central Peru, within the Upper Triassic-Lower Jurassic carbonate platform (Pucará Group) at the western margin of the Brazilian Shield. Production during the last 20 years and present reserves exceed 12 million tons of ore assaying about 12 percent Zn and 1 percent Pb. Sphalerite and galena, the only ore minerals, occur as lens-shaped bodies generally parallel to the bedding. Within the 1,400-m-thick Pucará sequence three ore-bearing dolomite units occur. The ore lenses are bound to dolomitized tidal flat and lagoon facies with cryptalgal lamination and evaporite molds and to adjacent oolithic grainstones of barrier facies.

Strontium, carbon, oxygen, and sulfur isotope geochemistry was carried out on consecutive crystallization generations. The results obtained display systematic trends. The $^{87}Sr/^{86}Sr$ ratios range between 0.7077 and 0.7084. The first generations display values very similar to those of Upper Triassic-Lower Jurassic ocean water. Later generations are slightly enriched in radiogenic strontium. The degree of enrichment in radiogenic strontium is low compared to other Mississippi Valley-type deposits. The $\delta^{18}O$ values range between −6 and −10 per mil PDB, and the $\delta^{13}C$ values between +2 and −1 per mil PDB. The late crystallization generations are enriched in the light isotopes of oxygen and carbon compared to the first generations. The sulfur isotope ratios of sphalerite are relatively homogeneous, ranging between 9.9 and 13.0 per mil. A trend to lighter sulfur isotope ratios with advancing diagenetic stage can also be recognized.

The San Vicente lead-zinc deposit formed during burial diagenesis. The temperatures indicated by sulfur isotope geothermometry (75°–92°C) would be consistent with temperatures reached at a burial depth of about 2 to 3 km. This might have been reached by the end of the Jurassic. A model based on abiogenic reduction of sulfates at or near the ore site, and the introduction of a zinc- and lead-bearing basinal brine characterized by strontium isotope ratios slightly higher than contemporaneous seawater and highly radiogenic lead, is favored. The association of the orebodies with peritidal facies with abundant sulfate molds is important evidence favoring the existence of two separate reservoirs for sulfur and metals. Leaching of detrital material derived from Precambrian upper crust from the Brazilian Shield would explain both strontium and lead isotope ratios.

Introduction

THE strata-bound Zn-Pb deposit of San Vicente (11°14′ lat S, 75°21′ long W, province of Chanchamayo, department of Junin) is located 328 km by road east of Lima, in the Chanchamayo area, 10 km south of San Ramón, in the tropical rain forest of the Ceja de Selva, which is the sub-Andean highland between the Andean cordillera and the Amazon forest (Fig. 1). San Vicente is the best known example of a belt of Zn-Pb-(Ba-F) deposits of the Mississippi Valley type in the eastern part of the Upper Triassic-Lower Jurassic Pucará basin. At present, it is the only mine in production.

Lead and zinc occurrences in Pucará rocks and as sulfide-bearing pebbles in rivers in the Chanchamayo area have been reported frequently since 1950. The Pichita Caluga lead-zinc deposit, 6 km northwest of San Ramón, was the first one to be mined (between 1951 and 1965 by the Compañía Minera Chanchamina, S.A). Amstutz (1956) reported on the carbonate-hosted María Esperanza lead mine, 11 km west of San Ramón, and compared it to the Missouri lead belt deposits. The San Vicente mine was staked by J. Carpena Monroy in 1955 which was the beginning of a small-scale lead operation. The Compañía Minera San Vicente was created in 1960 as a subsidiary of Mauricio Hochschild, S.A., and Compañía Minera Chanchamina. Subsequent exploration with participation of the Cerro de Pasco Corporation led to re-

* Present address: Department de Mineralogie, 13, rue des Maraichers, CH-1211 Geneve 4, Switzerland.

0361-0128/90/1132/1402-36$3.00

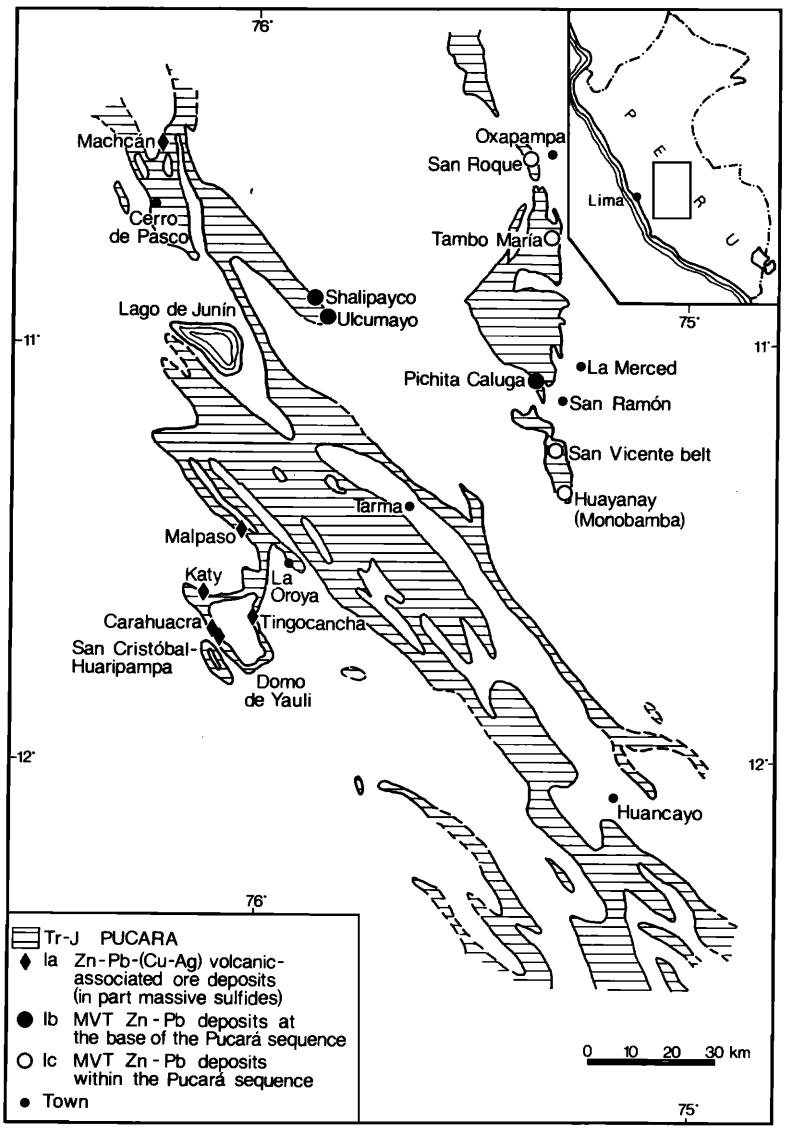

FIG. 1. Location of the San Vicente mine in an outcrop map of the Pucará Group. Geology according to Szekely and Grose (1972) and to the Japan International Cooperation Agency (1979) for the central and eastern parts of the basin, respectively. The location of the main Pucará-hosted strata-bound ore deposits is indicated (modified from Fontboté, 1990).

serves of 850,000 metric tons with 18 percent Zn. In 1969 the Compañía Minera San Ignacio de Morococha, S.A. (SIMSA) acquired partial control of the San Vicente deposit and by 1973 had total control. The present production is 3,000 metric tons/day, which makes San Vicente the largest zinc-producing mine in Peru. Accumulated production is about 6 million metric tons. Reserves exceed 5.1 million metric tons ore with a grade of 0.8 percent Pb and 12.6 percent Zn.

Aspects of the San Vicente mine have been discussed by Schulz (1971), Levin and Amstutz (1973), Levin (1975), Lavado (1980), Fontboté (1981), Fontboté et al. (1981), Gonzalez and Fontboté (1986), and Fontboté and Gorzawski (1988). This paper summarizes the geology, paleogeography, facies analyses, and trace element and isotopic (C, O, S and Sr) geochemistry of the San Vicente deposit. The formation of the ore deposit is studied in the frame of the diagenetic evolution of the host rock and of the evolution of the Pucará basin.

The Pucará Basin: An Extensive Carbonate Platform at the Beginning of the Andean Cycle

The Zn-Pb deposit of San Vicente is hosted by carbonate rocks belonging to the Upper Triassic-Lower

Jurassic Pucará Group. The Pucará basin developed as a wide carbonate platform at the western margin of the Brazilian Shield in northern and central Peru. The large extent and thickness of carbonate sediments deposited in peritidal environments makes the Pucará basin unique among the Andean basins. The mainly carbonate sediments of the Pucará Group represent a transgression over Paleozoic terranes and red-bed molasse series and alkaline and peralkaline lavas of the Mitu Group (Permian-Lower Triassic).

Regional aspects of the Pucará Group are described by Mégard (1968, 1978), Szekely and Grose (1972), Loughman and Hallam (1982), Prinz (1985a), and Fontboté (1990). Figure 2 shows a schematic correlation of selected stratigraphic sequences in the Pucará basin.

Important differences exist between the facies development in the eastern (sub-Andean zone and Eastern Cordillera) and in the central part of the Pucará basin (Altiplano region). As discussed by Fontboté (1990), the following two paleogeographic areas can be distinguished up to the Hettangian (Figs. 2 and 3). The first area is an eastern belt with extensive development of peritidal dolomites, in part with preevaporitic characteristics, deposited in sabkhalike facies. These most likely interfinger with clastic and evaporitic sediments sourced by the emerged Brazilian Shield (the Lower Sarayaquillo Formation as defined by Mégard, 1978). This eastern belt hosts the Zn-Pb deposits of San Vicente and Shalipayco, as well as numerous other carbonate-hosted Zn-Pb-(Ba) occurrences (Figs. 1 and 2). The second paleogeographic area is represented by the central Pucará basin. It also is characterized by neritic sediments, but in general terms, deposition occurred in relatively deeper environments than the time equivalents in the eastern Pucará basin. In Pliensbachian to Toarcian times shallow-water facies with increasing clastic components advanced from east to west and finally dominated the Pucará sedimentation in the entire basin.

Despite the different lithologic development in the eastern and in the central Pucará basin, similar facies trends can be traced in both parts (Fig. 2). The peritidal carbonate sequence of the Tambo María Formation (Upper Triassic-Hettangian, 600 m thick) correlates with the Chambará neritic carbonate rocks in the central Pucará basin. The bituminous shales and limestones of the Ulcumano Formation (Sinemurian,

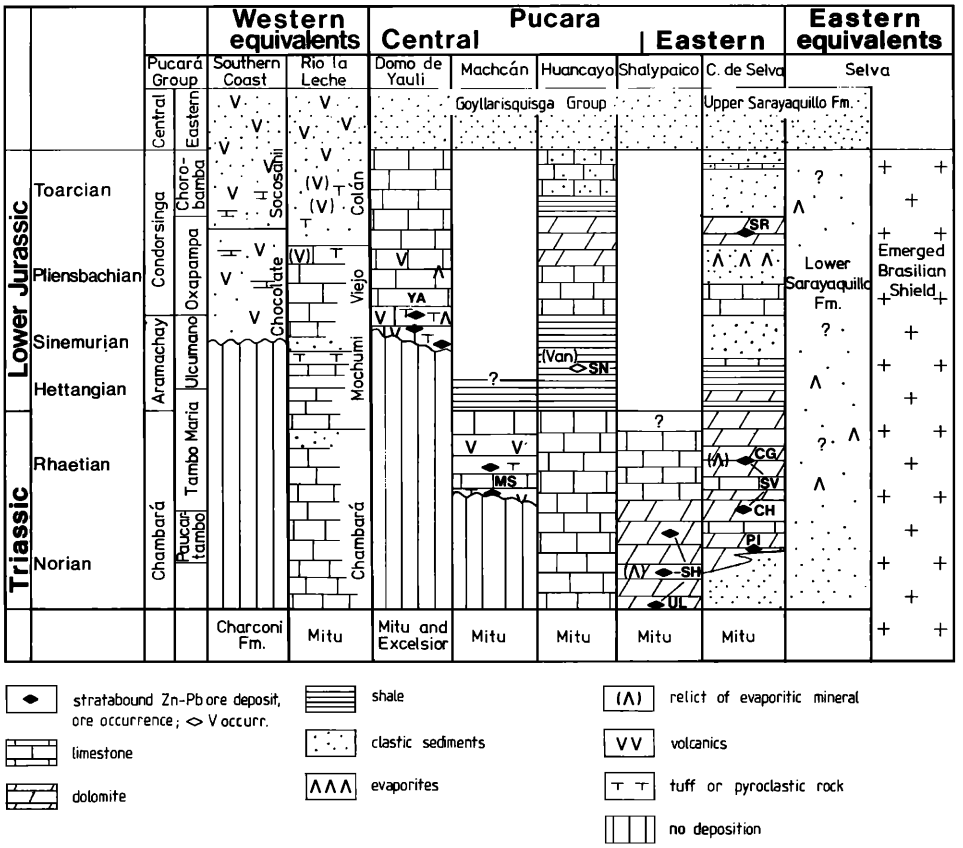

FIG. 2. Schematic correlation of selected stratigraphic sequences in the Pucará basin (from Fontboté, 1990).

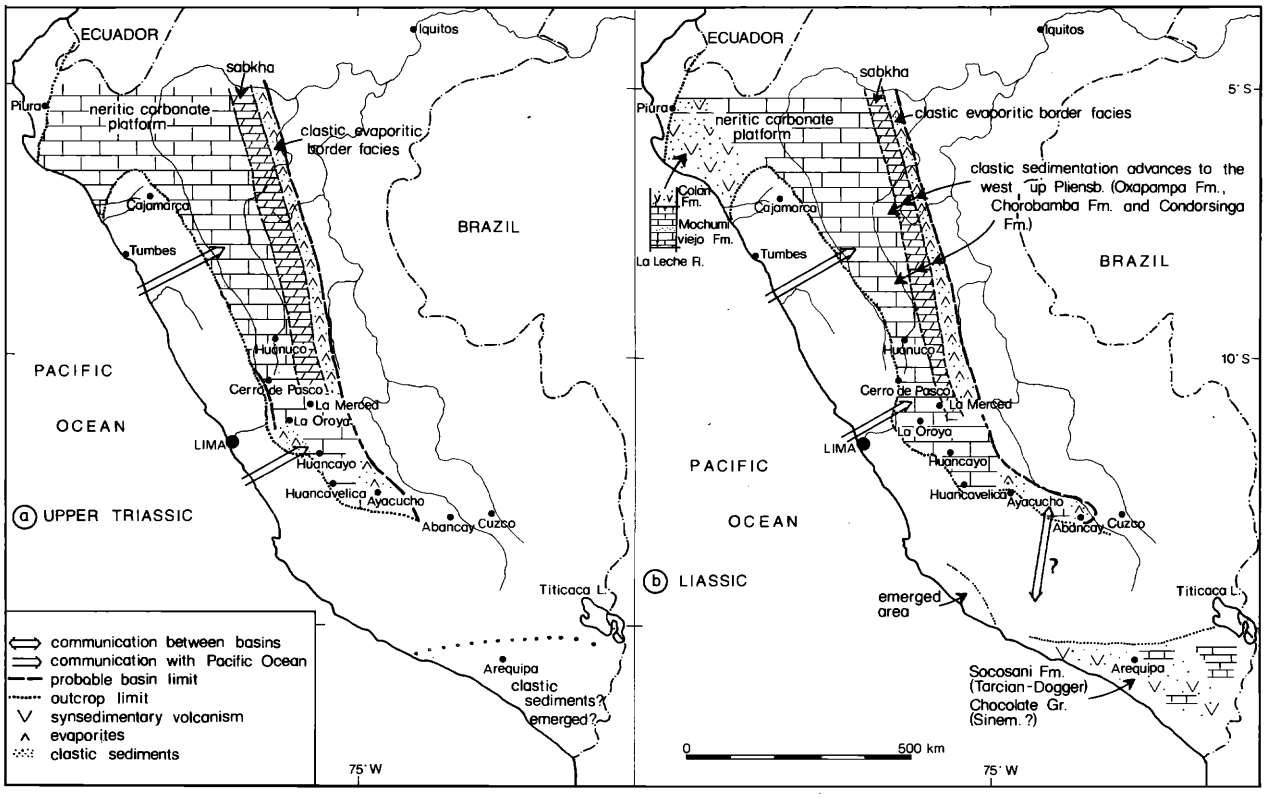

FIG. 3. Paleogeographic schemes of the Pucará basin during (a) the Upper Triassic, and (b) the Hettangian-Toarcian period (from Fontboté, 1990).

350 m thick) can be compared to the euxinic facies of the Aramachay Formation. The Oxapampa Formation (shallow-water dolomite and limestone, some gypsum and sandstone layers, 800 m thick) can be correlated with the regressive episode which characterizes the Condorsinga Formation.

The morphology of the western continuation of the Pucará basin remains uncertain because in the western Altiplano region possible Pucará sediments have been eroded in pre-Cretaceous times. A communication with the paleo-Pacific is documented in the Río de La Leche Valley (near 6° S) where an Upper Triassic-Lower Jurassic carbonate sequence similar to the Pucará sequence is described (Figs. 2 and 3; Pardo and Sanz, 1979; Pardo, 1983; Prinz, 1985a). It has been suggested that the Pucará basin was limited to the west by a subduction-related volcanic arc (Audebaud et al., 1973). Available evidence indicates that activity of a calc-alkaline volcanic arc started not earlier than Sinemurian-Toarcian times (Fontboté, 1990). This means that only the upper part of the western Pucará basin could have been influenced by a volcanic arc.

The evolutionary style of the eastern Pucará basin is more similar to that of carbonate platforms in pericratonic areas than to that of other Mesozoic Andean basins, which are often influenced by arc-related volcanism. The main similarities include rapid subsidence rates (probably favored by extensional block tectonics), the predominant carbonate sedimentation with extensive peritidal deposition and dolomite formation, and the location at the margin of an emerged continent.

Strata-Bound Ore Deposits in the Pucará Group

Different types of strata-bound ore deposits occur in sedimentary rocks of the Pucará Group (Dunin, 1975; Kobe, 1977, 1982; Dalheimer, 1990; Fontboté, 1990). In the western part of the basin volcanogenic and exhalative factors appear to predominate. This applies to the Zn-Pb(-Ag-Cu) deposits, in part with massive sulfide parageneses, located near the base of the Pucará Group in sequences with significant volcanic and/or volcaniclastic intercalations (e.g., Carahuacra, Huaripampa, and Manto Katy).

In the eastern part of the Pucará basin Mississippi Valley-type ore deposits prevail. The San Vicente and Shalipayco Zn-Pb deposits are the more important ones, but additional Zn-Pb-(F-Ba) occurrences and prospects are known along a north-south belt at least 200 km long (Fig. 1). They include undeveloped ore occurrences near Chaglla (lat 9°50′ S, long

75°48′ W, about 90 km north of Oxapampa), Oxapampa, Tambo María, and the Ulcumayo and Pichita Caluga mines, and several ore showings south of San Vicente (Fig. 1). Huayanay, 5 km south of Monobamba, is the southernmost known zinc-lead occurrence (Fig. 1; Tayler, 1962). Most of the occurrences are in dolomitic rocks, mainly in the Tambo María Formation.

The Eastern Cordillera and the sub-Andean region are fairly inaccessible and poorly known. The known ore deposits and occurrences and the persistence of facies and diagenetic characteristics indicate that a large Mississippi Valley-type province is located in the eastern Pucará basin. Therefore, this shallow-water carbonate platform at the western margin of the Brazilian Shield constitutes an interesting exploration target.

Regional Geology of the San Vicente Deposit

San Vicente is located between the Cordillera Oriental and the sub-Andean zone. Figure 4 gives an overview of the regional geology of the San Vicente mining area which integrates the data of Levin (1975), Capdevila et al. (1977), Mégard (1978), Japan International Cooperation Agency (1979), internal mine reports, and our own observations. The oldest stratigraphic unit is comprised of mica schists and gneisses and is assigned to the Precambrian. It is overlain by Paleozoic sediments, including carbonate rocks of the Permian Copacabana Group, and by sandstones and conglomerates of the Permian-Lower Triassic Mitu Group, which in this area consists mainly of terrestrial clastic sediments, in part volcaniclastic, but without the lavas observed in other parts of the Mitu Group. The transition between the Mitu and Pucará Groups in the San Vicente mining area will be discussed below. Carbonate rocks of the Pucará Group (up to 1,900 m thick) trace a north-south–trending belt. Dogger and Malm clastic rocks (the Upper Sarayaquillo Formation, about 1,000 m), as well as continental Cretaceous sediments (the Oriente Group, about 1,000 m and the Chonta Group, about 1,900 m), occur north of San Ramón. Tertiary (?) rhyolitic and ignimbritic flows are described by Levin (1975) in several localities near San Vicente, including one east of Vitoc (Fig. 4).

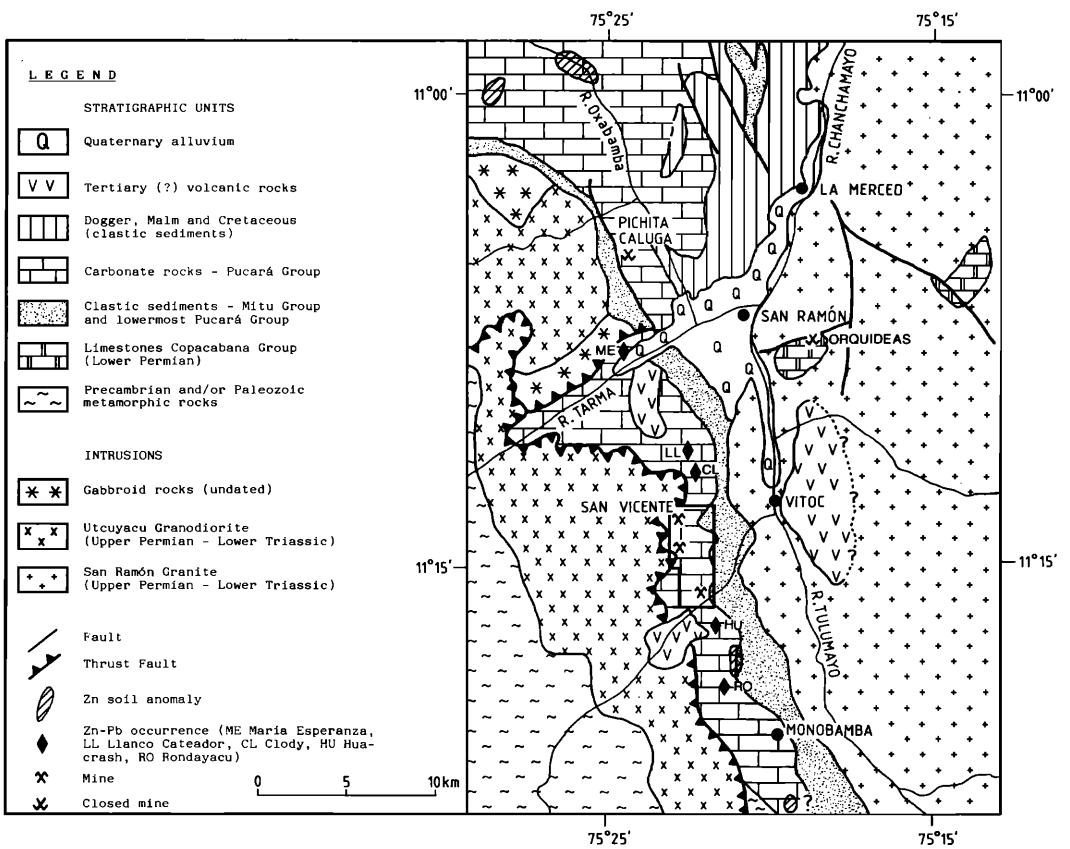

FIG. 4. Regional geologic map of the Chanchamayo area (compiled from Levin, 1975; Capdevila et al., 1977; Japan International Cooperation Agency, 1979; internal mine repts.; and our own observations). The location of the detailed map of San Vicente (Fig. 8) is indicated.

Three intrusive units are distinguished. The San Ramón (or La Merced) batholith occurs at the eastern part of the studied area (Fig. 4). It is made up of a red coarse-grained to porphyritic biotite-bearing granite which has been dated at 246 ± 10 Ma (Capdevila et al., 1977; Rb-Sr age recalculated according to Lancelot et al., 1978) and at 255 ± 1 Ma (Gunnesch et al., 1990). This uppermost Permian to lowermost Triassic age is consistent with the occurrence of pebbles of the red San Ramón granite in the Mitu Group conglomerates (for instance, near Vitoc). A K-Ar age determination of the pebbles themselves yields a similar age (238 ± 16 Ma; Japan International Cooperation Agency, 1976). The San Ramón batholith belongs to an extensive Permo-Triassic magmatic province in the Eastern Cordillera which areally coincides with the red-bed series and alkaline and peralkaline lavas of the Mitu Group. This geologic setting is interpreted as a Permo-Triassic ensialic rift zone (Kontak et al., 1985).

West of San Vicente a highly tectonized whitish biotite and hornblende granodiorite (Utcuyacu granodiorite) overthrusts the Pucará Group. This fault contact dips between 20° and 40° W and can be followed north-south for several kilometers (Fig. 4). The Utcuyacu granodiorite (in the mine reports also called "Tarma granite") was reported to intrude the Pucará rocks (Levin, 1975, p. 35) and therefore should have a Jurassic or Cretaceous age. As already noted by Capdevila et al. (1977), Levin's statement is questionable on the basis of additional field evidence. A Lower Triassic age (240 ± 4 Ma) of the Utcuyacu granodiorite as indicated by an Rb-Sr feldspar-biotite whole-rock isochron seems to be more realistic (Gunnesch et al., 1990).

Gabbroid and dioritic rocks represent the third intrusive unit in the area. Gabbroid rocks are reported north of the Tarma River in contact with the Utcuyacu granodiorite (Capdevila et al., 1977). Dioritic stocks intruding the Mitu and Pucará Groups have been described near the ore occurrence of Huacrash, south of San Vicente (Japan International Cooperation Agency, 1976). The altered subvolcanic and volcanic rocks, which intercalated with Pucará sediments at San Vicente (see below), could be correlated with these dioritic stocks.

Xenoliths of carbonate rocks occur within the San Ramón granite. These are well-bedded limestones often displaying contact metamorphic effects (as for example in the Orquideas mine, where garnets occur). They probably represent roof pendants of Copacabana limestone (Lower Permian).

San Vicente lies on the western limb of an anticline trending N 170° E. Numerous normal faults strike mainly N 50° E and N 140° E. In addition, the Utcuyacu overthrust fault is a major tectonic element. According to Mégard (1984) the first significant deformation phases affecting this area were the Quechua 1 and 2 phases (Oligocene and Miocene). However, overthrust faults like the Utcuyacu fault are typical for the Quechua 3 phase (upper Miocene).

The Pucará sequence in the San Vicente mining area

A clastic sequence corresponding in part to the Mitu Group underlies the Pucará carbonate rocks in the San Vicente area. The lowest horizons are yellow and brown sandstones and marls several hundred meters thick (Schulz, 1971). A red-violet horizon a few meters thick with arkosic sandstones and conglomerates follows. These conglomerates also contain the aforementioned pebbles of the San Ramón granite. The upper part of this clastic sequence has a characteristic red color and consists of sandstones and subordinate gypsiferous marls with a thickness of at least 100 m.

Figure 5 shows a generalized stratigraphic north-south cross section over 5 km in the San Vicente area. No discordance is observed between the red sandstones and the overlying thick Upper Triassic to Lower Jurassic carbonate sequence of the Pucará Group. In internal mine reports the "Red Sandstone" is usually included in the Permo-Triassic Mitu Group. However, Mégard (1978) indicates that frequently the lower part of the Pucará Group is detritic and is lithologically very similar to the Mitu Group. This is probably the case in San Vicente, as indicated by the transitional lithologic change of alternating beds of red sandstone and carbonate rocks over about 30 m (Schulz, 1971; Levin, 1974). The Red Sandstone immediately below the carbonate sequence should, therefore, be considered as part of the Pucará Group. It could also be considered to be an interdigitation of the Lower Sarayaquillo Formation. Thus the contact between the Mitu and Pucará groups would be located below this lithologic change, perhaps between the conglomerate level and the overlying red sandstone.

The carbonate sequence in the San Vicente mining area is up to 1,300 m thick and extends from Norian to Hettangian (Fig. 6). It strikes N 10° W and dips between 30° and 45° E (Fig. 7). The following lithologic units have been distinguished (the standardized stratigraphic heights used in Figure 6 and in all the tables, as well as the abbreviations used henceforth, are given in parentheses).

The Basal Series (BS, 0–442 m): This sequence consists of fine-grained limestone (mainly mudstone and wackestone[1]) and dolomite intercalations. There is abundant detrital material (up to 35% detritic quartz). The dolomitic beds coincide with the maxima of detrital material (González, 1987). This unit records the Upper Triassic transgression over the red

[1] Mudstone, wackestone, packstone, and grainstone according to the carbonate texture classification of Dunham (1962).

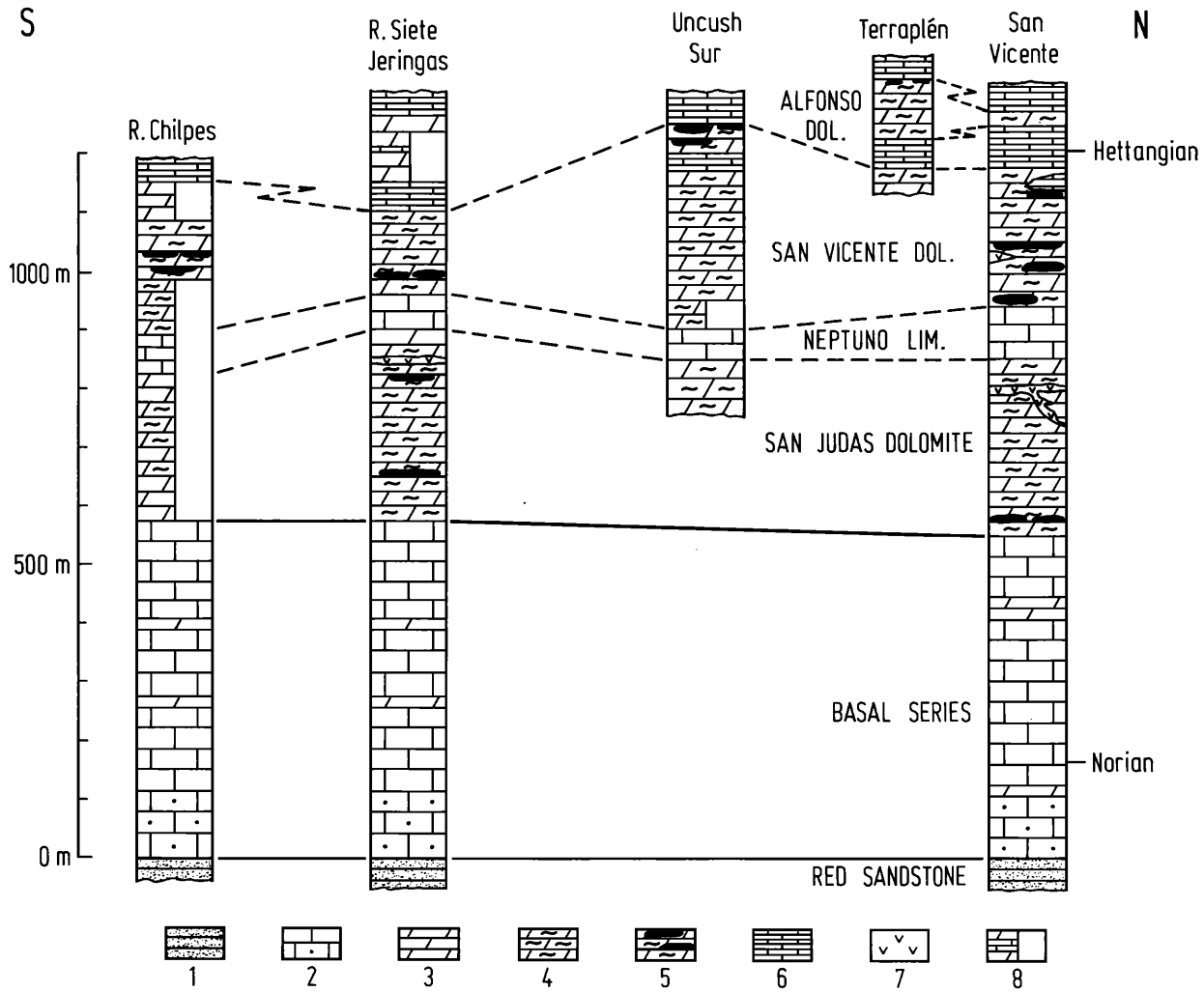

FIG. 5. Generalized stratigraphic sequences of the San Vicente area. The localities are indicated in Figure 8. 1 = red sandstone; 2 = limestone; 3 = dolomite; 4 = dolomite with diagenetic crystallization rhythmites and related structures; 5 = ore horizon; 6 = bituminous, laminated, silty limestone; 7 = volcanic and subvolcanic rocks, often wholly carbonatized; and 8 = poor exposure.

sandstone detrital facies at the base of the Pucará sequence. The depositional environments vary between coastal dolomitic facies with abundant detrital material and basinal facies with fine-grained limestone. In two samples from the upper part of this member small phosphate nodules have been detected with a microprobe. At the top of this member a slope breccia is recognized.

The San Judas Dolomite (SJD, 442–723m): This dolomite consists mainly of medium to coarsely crystalline dolomite. This is the first of three ore-bearing massive dolomite units displaying very similar petrographic and geochemical properties. It is characterized by the presence of abundant diagenetic crystallization rhythmites (formed by crystallization during diagenesis), geodelike textures, hydraulic breccias, diagenetic veinlets, and, in general, fabrics with megascopically distinguishable diagenetic crystallization generations. Despite the strong crystallization the original depositional fabric can often be recognized in thin section using the "light diffusor" described by Delgado (1977). The original textures are mainly oolitic packstone and grainstone (barrier facies). Detrital quartz is absent, except in the upper part.

The Neptuno Limestone (NL, 723–801m): This limestone is only partly dolomitized and serves as a field reference horizon in the San Vicente area. A detailed study of the Neptuno Limestone (González, 1987) has shown that this unit displays distinctive facies changes. The detrital proportion can reach up to 10 percent. The upper part of the Neptuno Limestone contains significant marl intercalations, probably including tuffaceous material. From top to bottom, the

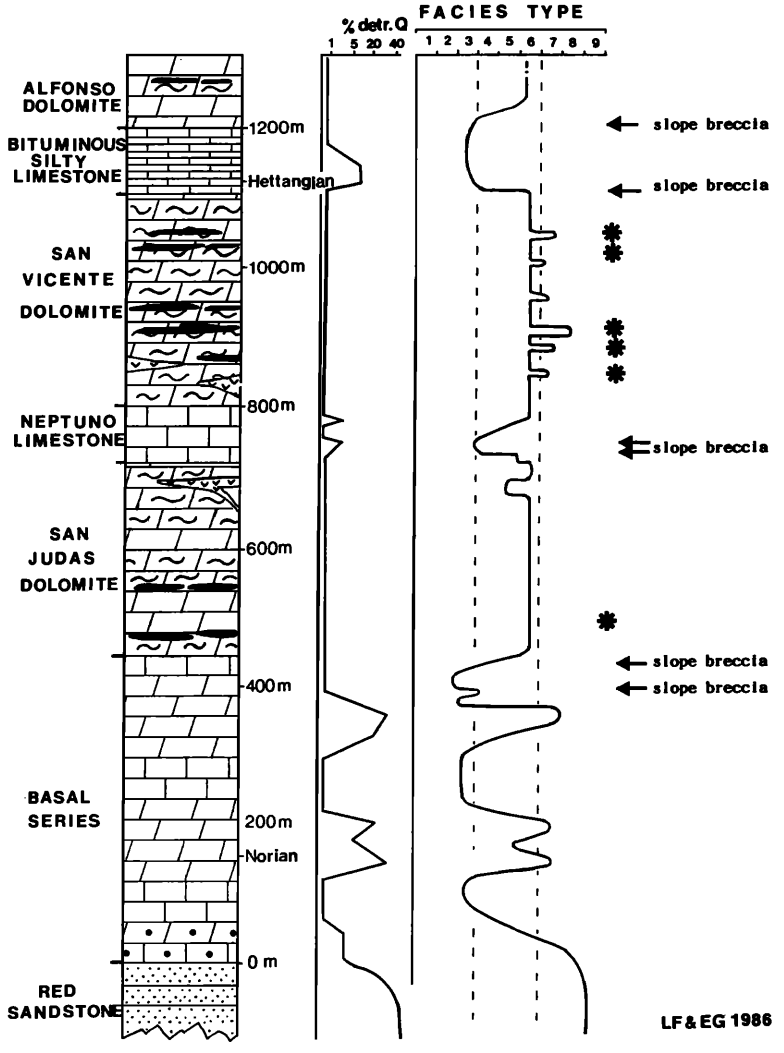

FIG. 6. Stratigraphic sequence in the San Vicente mine. Symbols as in Figure 5. Under facies type an evolution curve of the deposition environment has been represented (1 = open basin, 4 = slope; 5 = platform edge, 6 = barrier, 7 = lagoon, 8 = tidal flat, and 9 = continental). Star indicates occurrence of evaporites.

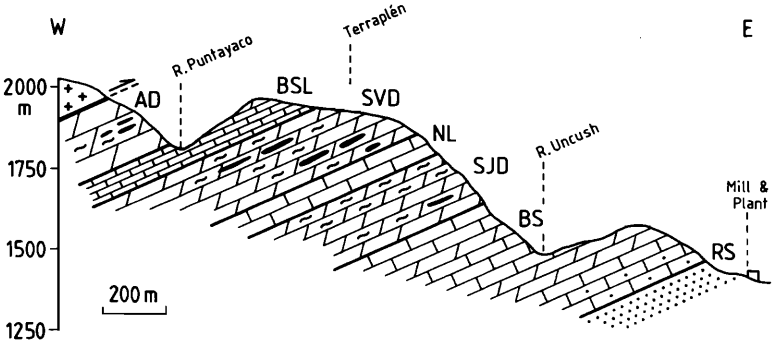

FIG. 7. Geologic east-west profile through the San Vicente mine. AD = Alfonso Dolomite; BSL = Bituminous Silty Limestone; SVD = San Vicente Dolomite; NL = Neptuno Limestone; SJD = San Judas Dolomite; BS = Basal Series; RS = Red Sandstone. Symbols as in Figure 5.

Neptuno Limestone comprises the following depositional environments: top—dolomitized barrier facies (San Vicente Dolomite), partly dolomitized barrier facies, foreslope in the basin facies, foreslope with slope breccias, and nondolomitized barrier facies; bottom—dolomitized barrier facies (San Judas Dolomite).

This documents a first collapse of the very constant platform sedimentation conditions which characterized the San Judas Dolomite.

The San Vicente Dolomite (SVD, 801–1,109m): This is the main ore-bearing unit. It is very similar to the San Judas Dolomite and consists mainly of dolomitized barrier calc-arenites (oolitic packstones to grainstones) with significant intercalations of bituminous, very fine to fine crystalline dolomite deposited in lagoon and tidal flat environments. These horizons are characterized by the occurrence of pellets, abundant algal mats, chert (in part chalcedony), and frequent evaporite molds. This member will be described later in more detail.

The Bituminous Silty Limestone (BSL, 1,109–1,189m): This unit is a bituminous, laminated, black limestone with shaly to silty intercalations. Abundant organic material occurs in thin bands and produces the characteristic lamination of this rock (total organic carbon between 0.74 and 1.59%; Lavado, 1980). The detrital proportion can be over 15 percent. The detrital grains consist almost exclusively of quartz, but some grains of tourmaline and white mica were also observed. The quartz grains are subangular to subroundish and range up to 200 μ in diameter. X-ray diffraction reveals that illite is the main mica mineral. Its abundant Hettangian ammonites have been described by Levin (1975) and Prinz (1985b).

The Bituminous Silty Limestone is a pyrite-rich hydrocarbon source rock (kerogene, type 2) characterized by the presence of abundant metabituminites indicating a very high evolution stage (meta-anthracite stage; Teichmüller, 1981, writ. commun.). This unit, with clear basinal facies, constitutes the second interruption of the carbonate platform sedimentation. The transitions toward platform sedimentation at the bottom (San Vicente Dolomite) and the top (Alfonso Dolomite) are marked by slope breccias.

The Alfonso Dolomite (AD, about 70 m in thickness): This unit is the third ore-bearing dolomite horizon and displays similar characteristics to the San Judas and San Vicente Dolomites. It was not studied in detail.

Tuffaceous, volcanic and/or subvolcanic intercalations occur in the upper part of the San Judas Dolomite, in the Neptuno Limestone, and in the lower part of the San Vicente Dolomite. Although they are generally almost completely carbonatized (see XRF analyses in Table 1) vesicular microlithic textures can be recognized frequently (Fontboté, 1981, p. 98).

TABLE 1. Ore Mantos in the North San Vicente Dolomite

Manto	San Vicente Dolomite (lower part) (m)	Whole carbonate sequence (m)
Jesus	160	961
Ayala	142	953
3t (techo = top)	122	923
3i (intermedio = intermediate)	95	896
3p (piso = bottom)	80	881
2	52	853

Levin (1975) describes an olivine basalt within the San Vicente Dolomite in a part of the San Vicente mine which is at present not accessible. The cross-cutting character of some of these volcanic rocks is clear (Fontboté, 1981). However, the presence of associated tuffaceous material could indicate that they are in part roughly coeval with the Pucará sediments.

Based on ammonite identifications, Prinz (1985b) dates the middle part of the Basal Series as Norian and the Bituminous Silty Limestone as Hettangian. In addition, the presence of Sinemurian in the area is proven by Prinz (1985b) on the basis of an *Arnioceras* found in a bituminous silty rock in a faulted block. Because of tectonic complications and poor outcrop conditions it cannot be elucidated if this bituminous facies belongs to the Bituminous Silty Limestone or to a similar unit above the Alfonso Dolomite.

Palacios (1980) defined a "Formación San Vicente" because a publication by Levin (1974) assigned a Ladinian age to the lower part of the Pucará carbonate rocks in San Vicente. Prinz (1985b) dismissed Levin's assumption and established that the carbonate sequence in San Vicente begins with the Norian, as in other parts of the Pucará basin, and consequently, the so-called "Formación San Vicente" of Palacios (1980) corresponds to the Paucartambo and Tambo María Formations (Norian-Hettangian).

Sedimentology of the dolomitic ore-bearing units

All three dolomitic units (the San Judas, San Vicente, and Alfonso Dolomites) are ore bearing and display very similar petrographic and geochemical characteristics. The main ore horizons occur within the San Vicente Dolomite (Figs. 5 and 8). The present study has shown that these three dolomite units were deposited in a peritidal platform comprising (1) the inner margin of the lagoon (tidal flat subenvironment) with partly preevaporitic conditions, (2) the lagoon sensu stricto, and (3) the outer margin of the lagoon (barrier subenvironment).

The barrier subenvironment predominates and is represented by completely dolomitized oolitic packstones and grainstones. The identification of these fa-

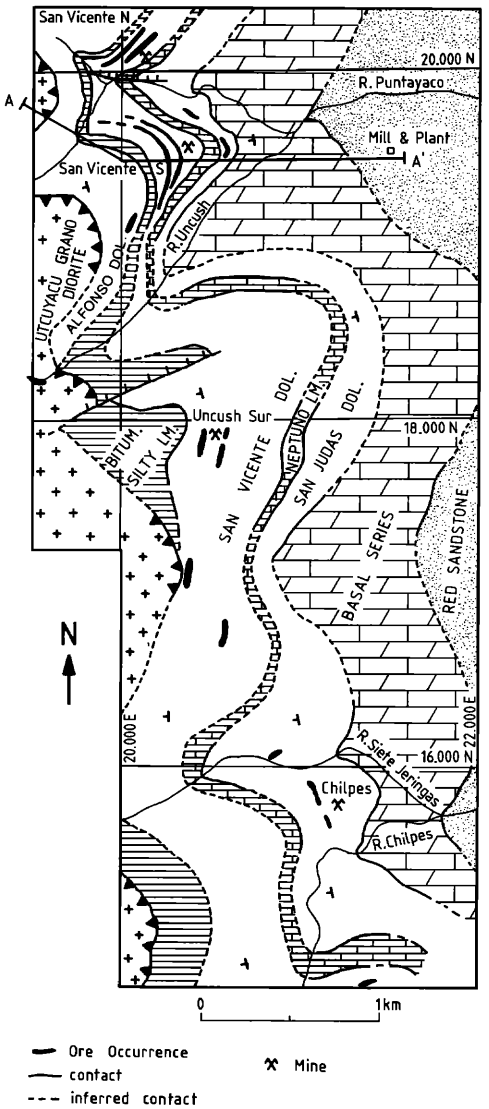

FIG. 8. Geologic map of the San Vicente mining area. A-A' = the profile in Figure 7.

cies is difficult because of the extensive dolomitization and recrystallization. Relict primary fabrics and dolomite grain size are used for this purpose. Figure 9b shows a typical example of dolomitized grainstone with a dolomite grain size of about 400 μ. The tidal flat and lagoon facies are characterized by very finely to finely crystalline dolomite with relict mudstone and pellet-grainstone fabrics that are difficult to recognize. Cryptalgal lamination (Fig. 10b and h) and evaporite molds (Fig. 11a–d) are frequent in tidal flat facies. Small pyrite grains occur intergranularly and in the frequent stylolite seams. The tidal flat and lagoon facies dolomite is very dark, almost black, due to its small grain size and the presence of abundant finely disseminated inclusions of organic matter. Medium to coarsely crystalline dolomite of calcarenitic barrier facies is lighter in color (gray to dark gray).

Total organic carbon analyses give values up to 3.46 percent (Lavado, 1980). Part of the organic carbon occurs as schlieren between dolomite grains and part as massive patches of bitumen in geodelike cavities. Detrital particles are extremely rare. Insoluble residues in dolomite include mainly quartz, in part as chert, and subordinate illite.

One interesting geochemical characteristic is the low Sr content of all three dolomitic units compared with the Sr contents of the limestones of the Basal Series or of the Bituminous Silty Limestone (see below). This may indicate early diagenetic dolomitization.

Detailed sedimentologic work (González, 1987; Fontboté and Gorzawski, 1987) suggests that in the San Vicente Dolomite there is a strong association between the occurrence of ore and certain host-rock facies. The dolomitic horizons hosting the orebodies consist mainly of barrier calcarenites. However, the ore lenses do not occur randomly in all parts of the barrier calcarenites. They show a clear link with intercalations of fine-grained dolomite with cryptalgal lamination and molds of evaporites attributed to tidal flat and lagoon facies.

Basin evolution and paleogeographic setting within the Pucará basin

At a regional scale the San Vicente ore deposit occupies a characteristic paleogeographic position at the edge of the Pucará basin, which is common with other similar ore occurrences in the eastern Pucará and comparable also to that of other Mississippi Valley-type deposits. The San Vicente ore occurs in dolomitic units deposited in evaporite-bearing peritidal environments located at the western margin of the Brazilian Shield.

The lithostratigraphic sequence of San Vicente presents two parts which correspond to different types of basin evolution. The lower part can be assigned to the Paucartambo Formation and is a typical transgressive sequence which ranges from continental sedimentation (red sandstone) to marine conditions with carbonate deposition and relatively abundant detrital material (basal series). The dolomitic portions of this unit coincide with maximum amounts of terrigenous particles and probably correspond to a shore environment. In general the limestones (mudstone and wackestone) represent subtidal to basinal facies.

The upper part of the sequence, which can be included in the Tambo María Formation, comprises three units deposited on a peritidal carbonate platform virtually free of detrital components (the San Judas, San Vicente, and Alfonso Dolomites). They are separated by two episodes of deeper water sedimen-

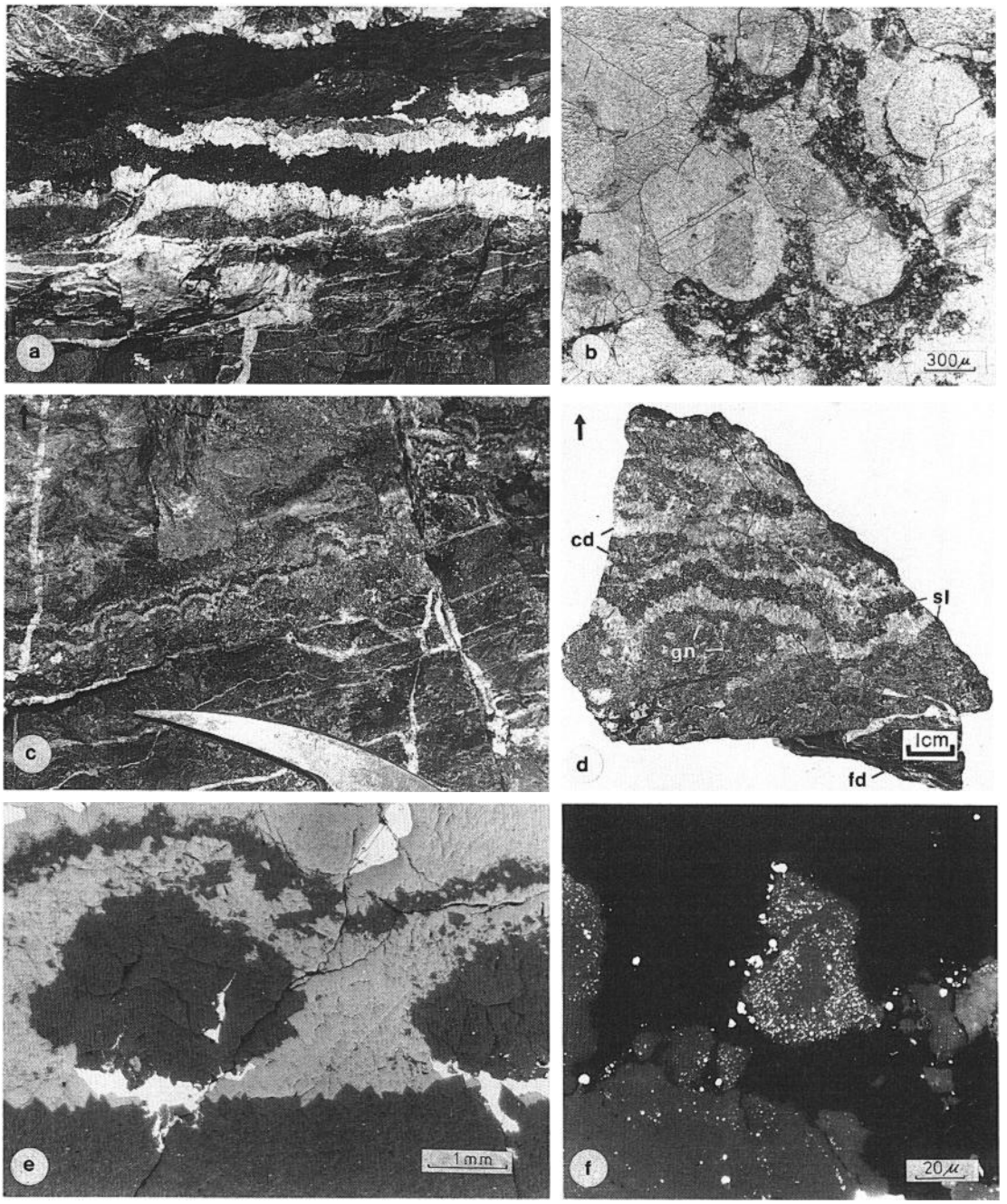

FIG. 9. a. Massive bitumen (black) in generation III of a geodelike cavity. Note the idiomorphic terminations of the dolomite crystals of generation II (white) toward the massive bitumen. The dark gray parts are fine to medium crystalline dolomite with dispersed organic matter (height 20 cm, sublevel 1,630 N, ramp 235 S). b. Thin section (parallel nicols sample FSV-49) of a dolomitic diagenetic crystallization rhythmite from generation I. The oolithic grainstone fabric is still recognizable. Note the disseminated organic matter (gray). c. and d. Mine wall and hand specimen views (sublevel 1,640 N, crosscut 530 E, sample FSV-10a) of a sulfide layer displaying sequence repetitions (fd = finely crystalline dolomite, cd = coarsely crystalline dolomite, sl = sphalerite, gn = galena). e. Polished section (parallel nicols, air, sample FSV-44) of a similar sulfide layer. Note the lack of corrosion between dolomite (dark gray) and sphalerite (light gray). Galena is white. f. Disseminated, very fine inclusions of pyrite in sphalerite (parallel nicols, oil, sample FSV-10a). This sphalerite presents obvious problems in separation by flotation.

tation (the Neptuno and Bituminous Silty Limestones). The transition from platform to basin sedimentation is clearly indicated by slope breccias. It appears therefore that the three dolomite ore-bearing units represent a cyclic repetition of large-scale tidal flat, lagoon, and barrier sedimentation on a platform separated by episodes of deeper sedimentation. A dynamic model explaining this evolution is shown in Figure 12. The peritidal facies belong to the shallow-water carbonate platform mentioned above, which developed in the eastern part of the Pucará basin (at the edge of the Brazilian Shield).

Although in the San Vicente area units stratigraphically above the Tambo María Formation are not known because of the overthrust of the Utcuyacu granodiorite, it is assumed from regional comparisons that marine Pucará sediments with a thickness of about 1,200 m formed up to the Toarcian (Ulcumano, Oxapampa, and Chorobamba Formations). Subsequent clastic sediments of the Upper Sarayaquillo Formation (Middle to Upper Jurassic) resulted in a burial depth exceeding 2,000 m. By the end of the Jurassic the former Pucará basin was dissected by the uplift of the north-south–trending Marañón geoanticline. Continental Cretaceous sediments (the Oriente Group, about 1,000 m, and the Chonta Group, about 1,900 m) increased the burial depth to about 5,000 m before the Quechua 1 and 2 deformation phases, which affected the Eastern Cordillera and sub-Andean region in Oligocene and Miocene times (Mégard, 1984).

Ore Occurrences

The San Vicente Dolomite is the main ore-bearing unit. It hosts the exploited part of the San Vicente mine, as well as other ore occurrences to the north (Clody) and south of the San Vicente mine (particularly visible in profiles along the Río Chilpes and the Río Siete Jeringas and in Uncush Sur, Figs. 4, 5, and 8). Other ore occurrences are located in the San Judas Dolomite (Chilpes prospect, San Judas mantos) and in the Alfonso Dolomite (Alfonso mantos). Ore showings with uncertain stratigraphic position are known in (from north to south) Llanco Cateador (northwest of Vitoc), at the Huacrash Hill, in the Rondayacu Valley, and north and south of Monobamba (Figs. 1 and 4).

The ore paragenesis is very simple with sphalerite and galena as the only ore minerals. The Zn content may range up to 30 percent. The average grades of the ore are 11.8 percent Zn and 0.8 percent Pb, respectively. Pyrite forms part of the paragenesis, but is always present in very small amounts, except in one horizon of the Chilpes prospect where it occurs in two massive layers a few centimeters thick within fault planes. Traces of marcasite, chalcopyrite, bournonite, and other sulfosalts are present. Fluorite and barite are reported by Levin (1975). This simple paragenesis, typical of Mississippi Valley-type deposits, differs significantly from the Pucará-hosted ore deposits associated with igneous activity (e.g., Huaripampa and Carahuacra).

The ore in the San Vicente mine forms lens-shaped bodies located in certain horizons (Fig. 13). These horizons, containing one or more lens-shaped bodies, are called mantos. The lens-shaped orebodies are in general parallel to the stratification and do not display a great lateral continuity; the maximum length of a single ore lens rarely extends over 300 m. Mine reports indicate that the maximum elongation of the ore lenses is usually north-south. Their thickness ranges between a few decimeters and a few meters. The top and bottom contacts of the high-grade lenses with the enclosing dolomite are sharp. The mantos in the northern part of the San Vicente mine are given in Table 1.

The ore lenses are locally affected by several normal faults. The most important faults strike N 45°–50° E and N 130°–150° E. Recent karst dissolution has produced major unconsolidated collapse breccias containing important amounts of ore (Fig. 13).

Ore Textures and Structures

Rhythmic structures

A large part of the San Vicente ore displays a characteristic rhythmic banding (Fig. 10a–h). It is locally known as "estructuras cebra." These structures are comparable to fabrics observed in numerous carbonate-hosted ore deposits and also in dolomitic rocks not directly associated with ore deposits. They are generally referred to as "zebra ore" or "zebra rock," but many other local names are also used (e.g., "coontail" ore in southern Illinois; "franciscana" in southern Spain; and "mineral rubanné" in the French literature). Because the rhythmicity is basically not inherited from an original sedimentary rhythmicity but rather created by a process of crystallization and recrystallization, often during diagenesis, the terms "crystallization rhythmite" and "diagenetic crystallization rhythmite (DCR)" have been proposed (Fontboté, 1981; Fontboté and Amstutz, 1983).

The term diagenesis includes late diagenesis, i.e., processes taking place under considerable burial. In fact, diagenetic crystallization rhythmites appear to be in most cases a product of burial diagenesis. In earlier stages of the investigation (Fontboté and Amstutz, 1983) the working hypothesis was proposed that the rhythmites reflect a process of differentiation by crystallization fractionation during diagenesis in the sense of Amstutz and Park (1971). Detailed geochemical work carried out on rhythmites of numerous localities around the world (Fontboté and Gorzawski, 1987; Gorzawski et al., 1989) only supports certain

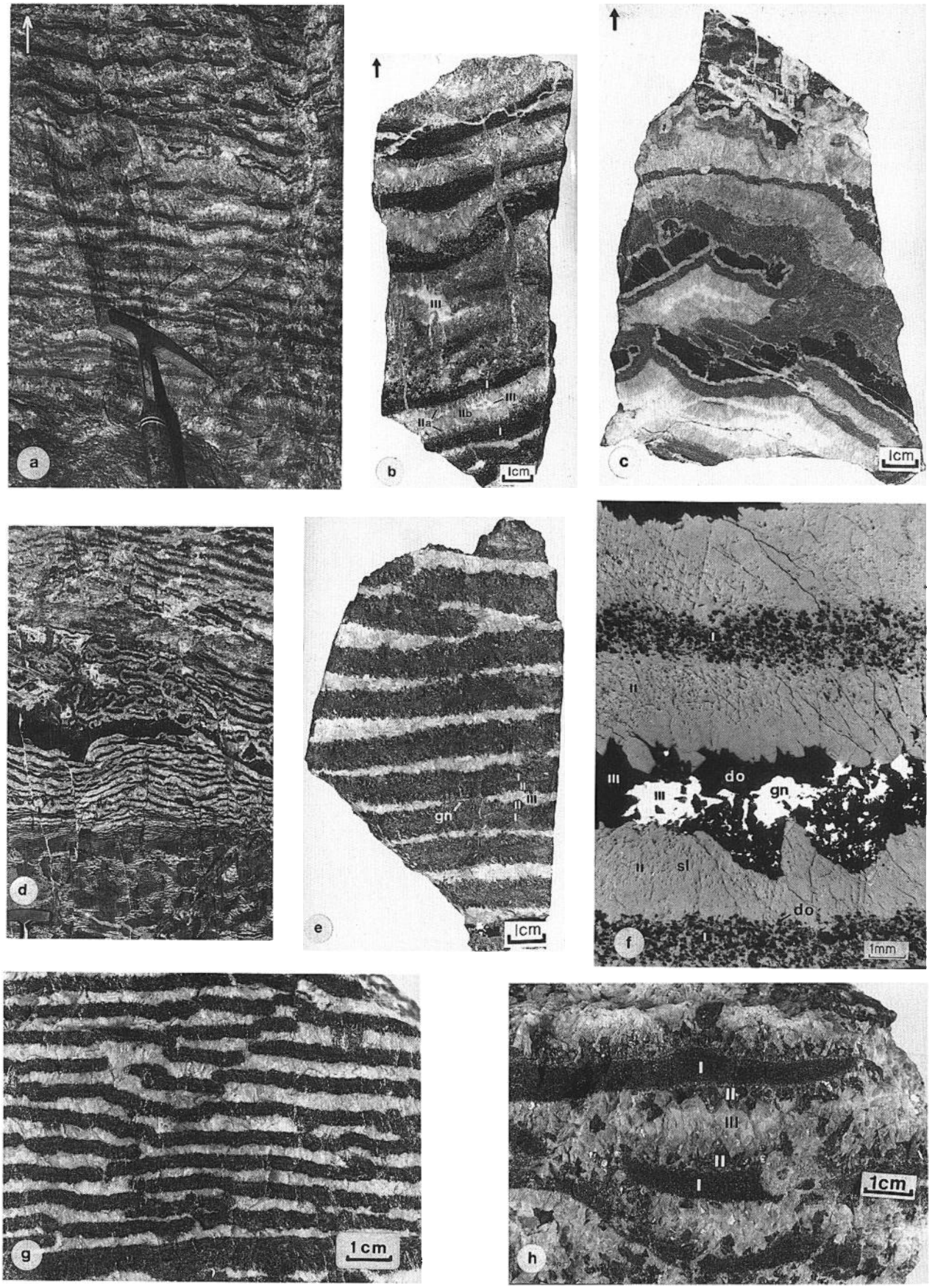
a
b
III
I
III
IIa
IIb
I
1cm
c
1cm
d
e
I
II
III
II
I
gn
1cm
f
I
II
III
do
III
gn
II
sl
do
I
1mm
g
1 cm
h
I
II
III
II
I
1cm

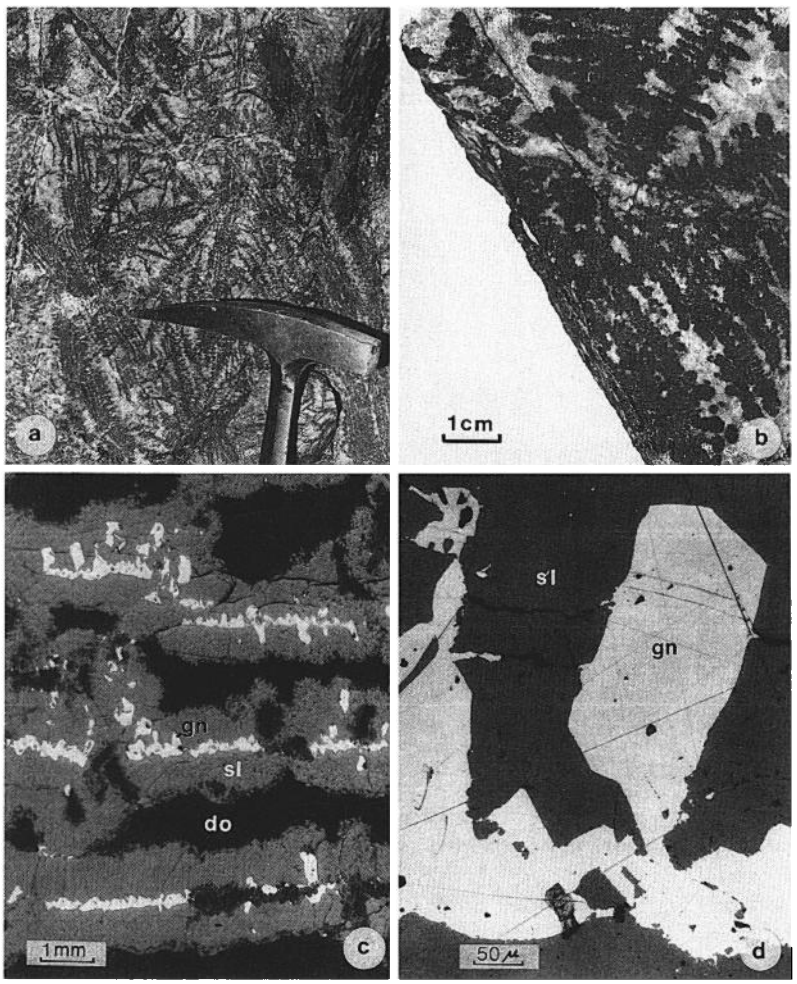

FIG. 11. Reticulate texture of galena (gn) and sphalerite (sl) in dolomite (do); evidence of vanished evaporites (1,452 N level, gallery 405). a. View of mine wall. The dark parts consist of sphalerite and galena, the light parts of dolomite. b. Hand specimen view. c. and d. Polished sections (parallel nicols, air). Galena clearly displays pseudomorphic textures after a sulfate mineral, probably gypsum. This is particularly clear in photo (d) which is an enlargement of the upper left area of (c).

aspects of this hypothesis. In particular, it appears that the process generally is not isochemical and includes dissolution and replacement phenomena. The rhythmites described in the present work are thought to have formed during late stages of diagenesis, under a burial of about two to three kilometers, by a reaction

FIG. 10. Diagenetic crystallization rhythmites of San Vicente. a. Mine wall (manto Ayala, 1,652 N level, ramp 360). b. Hand specimen (sample FSV-60) of diagenetic crystallization rhythmites from the same exposure shown in (a). The dark bands (generation I) consist of fine-grained sphalerite and dolomite with disseminated organic matter. Cryptalgal lamination is still recognizable. The bipolar growth of yellow sphalerite (IIa), in part geopetal, can be easily distinguished. Two generations of dolomite (IIb and III) are visible. c. Hand specimen (sample FSV-44) showing a complex texture with some repetitions in the crystallization sequence and dissolution features. d. Mine wall with another aspect of the manto Ayala (1652 N level, ramp 360). The lower part of the photo consists of dolomitic diagenetic crystallization rhythmites. The upper part shows a transition between orbicularlike and rhythmic ore textures. e. Hand specimen of diagenetic crystallization rhythmite ore (sample FSV-I). f. Polished section (parallel nicols, air) of the sample shown in (e). I = dark fine-grained sphalerite (sl) and dolomite (do), II = brown sphalerite, and III = sparry dolomite and occasionally galena (gn). g. Hand specimen of diagenetic crystallization rhythmite ore showing high periodicity. h. Same sample, detail of the three generations forming a diagenetic crystallization rhythmite: I = fine-grained sphalerite and dolomite with algal lamination, II = brown-yellow sphalerite, and III = sparry dolomite.

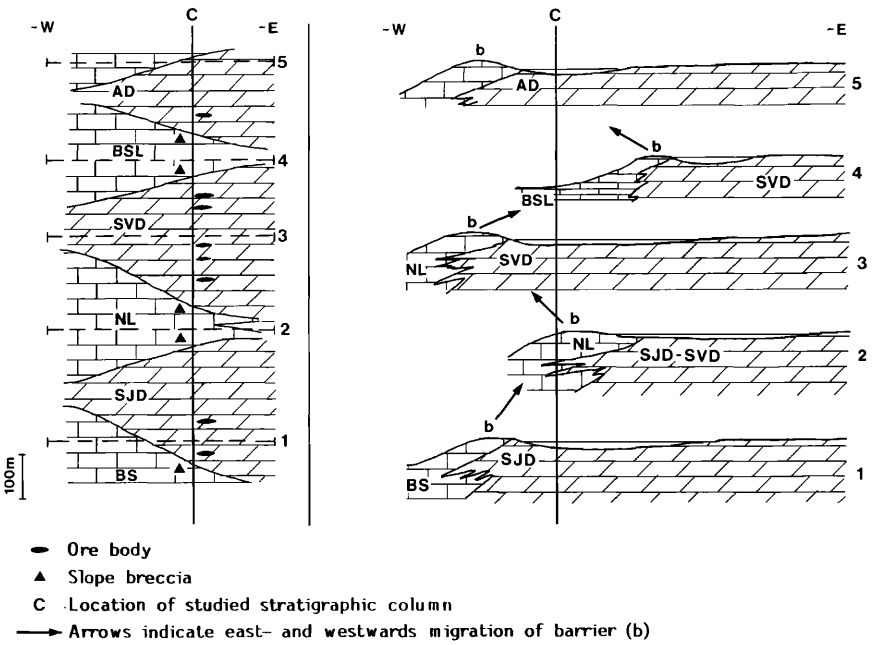

FIG. 12. Dynamic model explaining the development of the carbonate platform in the San Vicente area.

of the original carbonate rock with an influxing basinal brine.

Crystallization rhythmites can also be produced by processes other than burial diagenesis and in other than sedimentary environments. For example, similar rhythmic banded structures are also produced by metamorphic or magmatic crystallization and recrystallization.

In the diagenetic crystallization rhythmites from San Vicente and other localities it is possible to recognize two or three consecutive crystallization generations megascopically. On the basis of geometric criteria the following three generations are distinguished, with dolomite, sphalerite, and galena as the main minerals (see also Fig. 10e–h and Table 2).

Generation I: This generation is a dark, fine- to medium-grained aggregate of dolomite with or without sphalerite with numerous disseminated opaque inclusions (mainly organic carbon, subordinate pyrite) within and between the grains. The small grain size and the abundant opaque inclusions yield dark colors even in the cases in which this generation consists of dolomite. Although generation I is essentially a recrystallization product, relict primary depositional features like oolitic grainstone fabric (Fig. 9b) or cryptalgal lamination (Fig. 10b) can be still recognized in places.

Generation II: This generation consists of coarse or very coarse subhedral crystals of dolomite and/or sphalerite arranged in a bipolar pattern, growing above and below generation I (Fig. 10f). The limit between generations I and II is gradational in detail, often displaying dissolution patterns. In contrast to generation I, generation II contains few opaque inclusions and is therefore usually light colored. Zonal crystal growth is often recognized. Geopetal features are frequent. For example in Figure 10b, c, and h, it can be seen that generation II sphalerite is better developed above than below the bands of generation I. Several subgenerations are often observed (Fig. 10b).

Generation III: This generation consists of the remaining central space or its xenomorphous filling, which is coarse- or very coarse grained dolomite or galena (Fig. 10e and f). Occasionally it consists of calcite or massive bitumen (Fig. 9a). The contact between generations II and III does not show dissolution features and is sharp in detail (Fig. 10f). The antipolar crystals of generation II are often in direct contact and then generation III is missing.

Inasmuch as these generations are distinguished using geometric criteria, a strict time correlation between different parts of the deposit may not be correct but constitutes a first approximation.

Diagenetic crystallization rhythmites consisting of dolomite also occur in ore-free parts of the San Judas, San Vicente, and Alfonso Dolomite units. As in other ore districts, they have been used as an empirical exploration guide because of their frequent association with ore minerals. They reveal the interaction between a fluid and a sedimentary rock, usually carbon-

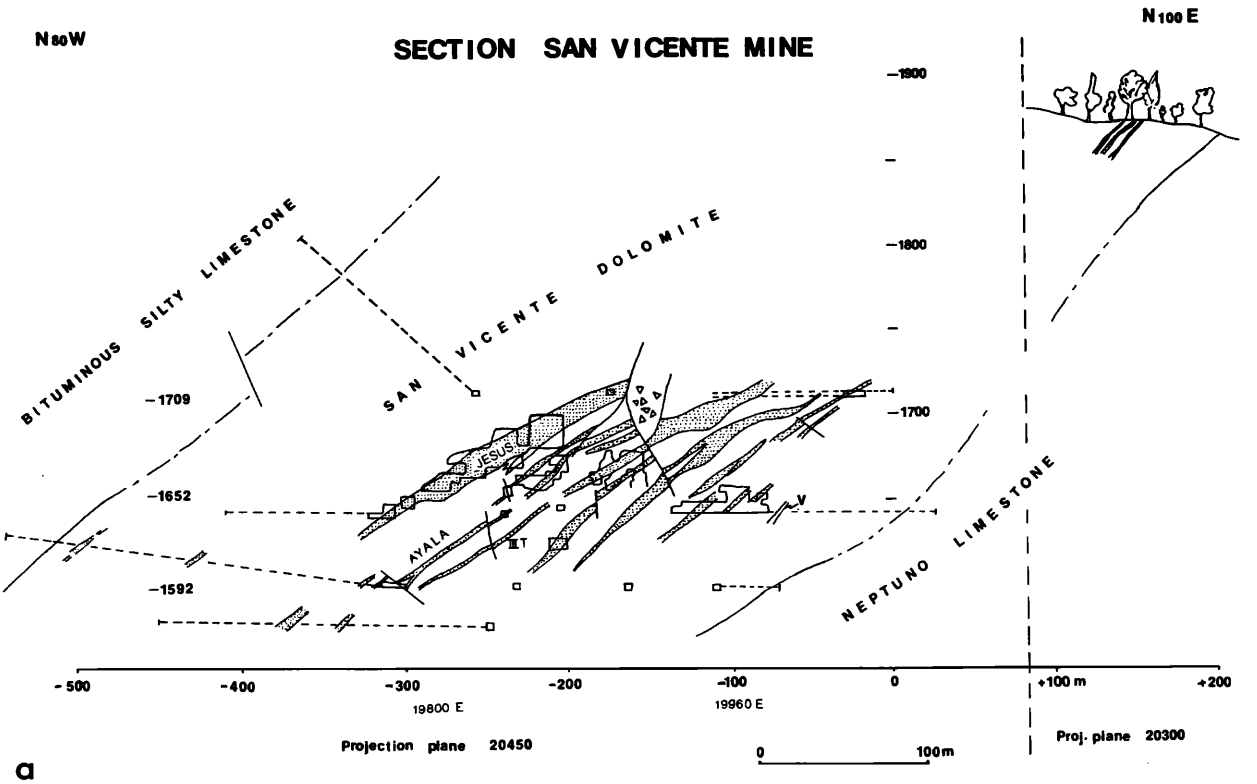

a

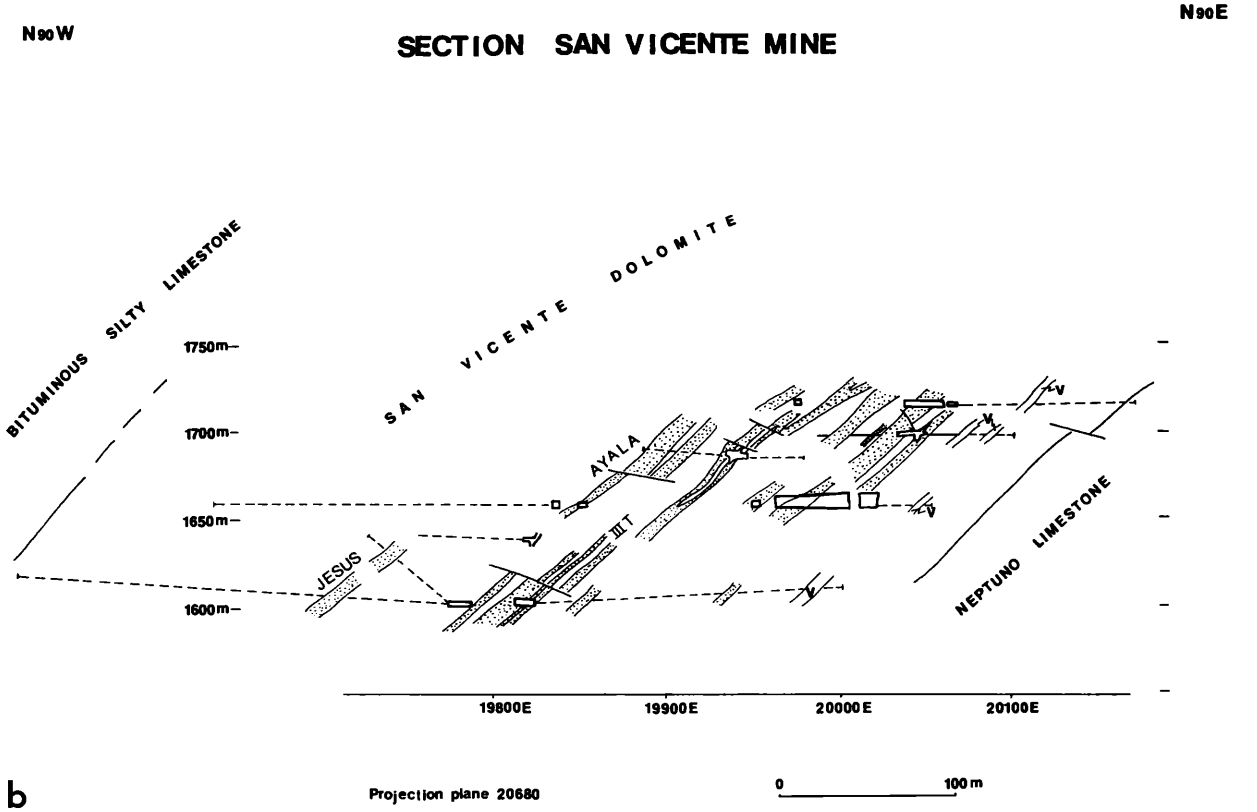

b

FIG. 13. a. and b. Representative east-west sections of the San Vicente mine projected onto the projection planes 20450 and 20680.

TABLE 2. Composition of Representative Examples of Diagenetic Crystallization Rhythmites from San Vicente

Sample \ Generation	I	II		III
		IIa	IIb	
FSV-I	Sphalerite + dolomite [Pyrite (a) and (b)]	Dark brown sphalerite [Pyrite (a) and (c) + marcasite (a) and (c)]	Light brown sphalerite	Dolomite + galena
FSV-60	Dolomite + sphalerite {Pyrite (a)}	Yellow sphalerite	Gray dolomite	White dolomite
SV-7	Sphalerite + dolomite [Authigenic quartz] {Pyrite (a)}	Brown sphalerite	Yellow sphalerite	Dolomite + galena {Pyrite (a)}
SV-41	Dolomite + sphalerite [Pyrite (a) and (c)]	Dark brown sphalerite [Pyrite (c)]		Dolomite {Pyrite (a)}
SV-41 a	Sphalerite (ca. 75%) + dolomite [Pyrite (a)]	Dark brown sphalerite {Pyrite (a)}		Dolomite or occasionally massive pyrite

Abbreviations: (a) = euhedral to subhedral grains ranging between 1 and 10 μ in size, occasionally up to 100 μ; (b) = very small inclusions disseminated in sphalerite; (c) = small inclusions oriented along crystallographic directions in sphalerite; [ ] = accessory mineral; { } = very small amount

atic, resulting in dissolution, recrystallization, and crystallization of new phases. The characteristics of such a fluid in San Vicente are discussed later.

Other structures

Generations comparable to those in diagenetic crystallization rhythmites are also recognized in other fabrics not displaying a rhythmic banding. They include orbicularlike and cockade structures (Figs. 10d and 14a).

Various fabrics indicate an overpressure regime during crystallization from the ore fluid. Among these are hydraulic breccias, upward veins, and tepeelike structures. Several parts of the San Vicente Dolomite have hydraulic breccias with fragments of dark fine- to medium-grained dolomite rimmed by subhedral coarsely crystalline dolomite (Fig. 14e and f). The breccia matrix consists of sparry dolomite and often contains spots of massive bitumen in geodelike cavities. Brecciated ore fragments occur in a few places, but ore minerals generally do not crystallize in the matrix of the breccia. The hydraulic breccias are considered to have originated through breaking and dissolution of dolomite under overpressure conditions. This is supported by their frequent occurrence in horizons parallel to the bedding and by their association with crosscutting veins produced by escaping solutions. The prevailing overpressure regime is clearly documented in Figure 14b, which shows one such crosscutting vein above a breccia horizon located under a layer of dark dolomite. In places, crosscutting veins break dolomite layers producing tepeelike structures that are always oriented upward (Fig. 14c and d).

The former presence of evaporite minerals is well documented in several parts of San Vicente, especially in manto 3t (Table 1). The most common evidence consists of pseudomorphs of coarsely crystalline dolomite after gypsum nodules in dolomitized algal mat laminated wackestones and mudstones. Spectacular examples of pseudomorphic textures after sulfate minerals are the reticulate textures of galena in sphalerite and dolomite shown in Figure 11a to d.

Paragenetic sequence

The paragenetic sequence of San Vicente can be studied easily in the megascopically observed crystallization generations of the rhythmites and related fabrics, as well as in hydraulic breccias and in crosscutting veins. The paragenetic sequence is simple and constant throughout the deposit. It can be summarized in each of the generations as follows: (I) medium crystalline dolomite and sphalerite, (II) sphalerite or sparry dolomite, and (III) galena or sparry dolomite and subordinate massive bitumen and calcite. The paragenetic sequence observed in rhythmites is shown in more detail in Figure 15.

Scarce pyrite crystallizes in generation I, mainly as very small grains, which are in part euhedral. In generation II, pyrite is still less frequent and forms small inclusions in sphalerite and dolomite. Sometimes the inclusions of pyrite and also of marcasite follow crystallographic planes in sphalerite of generation II. A thin rim of small euhedral pyrite crystals occurs sometimes at the border between sphalerite II and dolomite III. In generation III, only very sparse and small grains of pyrite are observed. Pyrite occurs in places as very abundant and very small (1–0.1 μ) in-

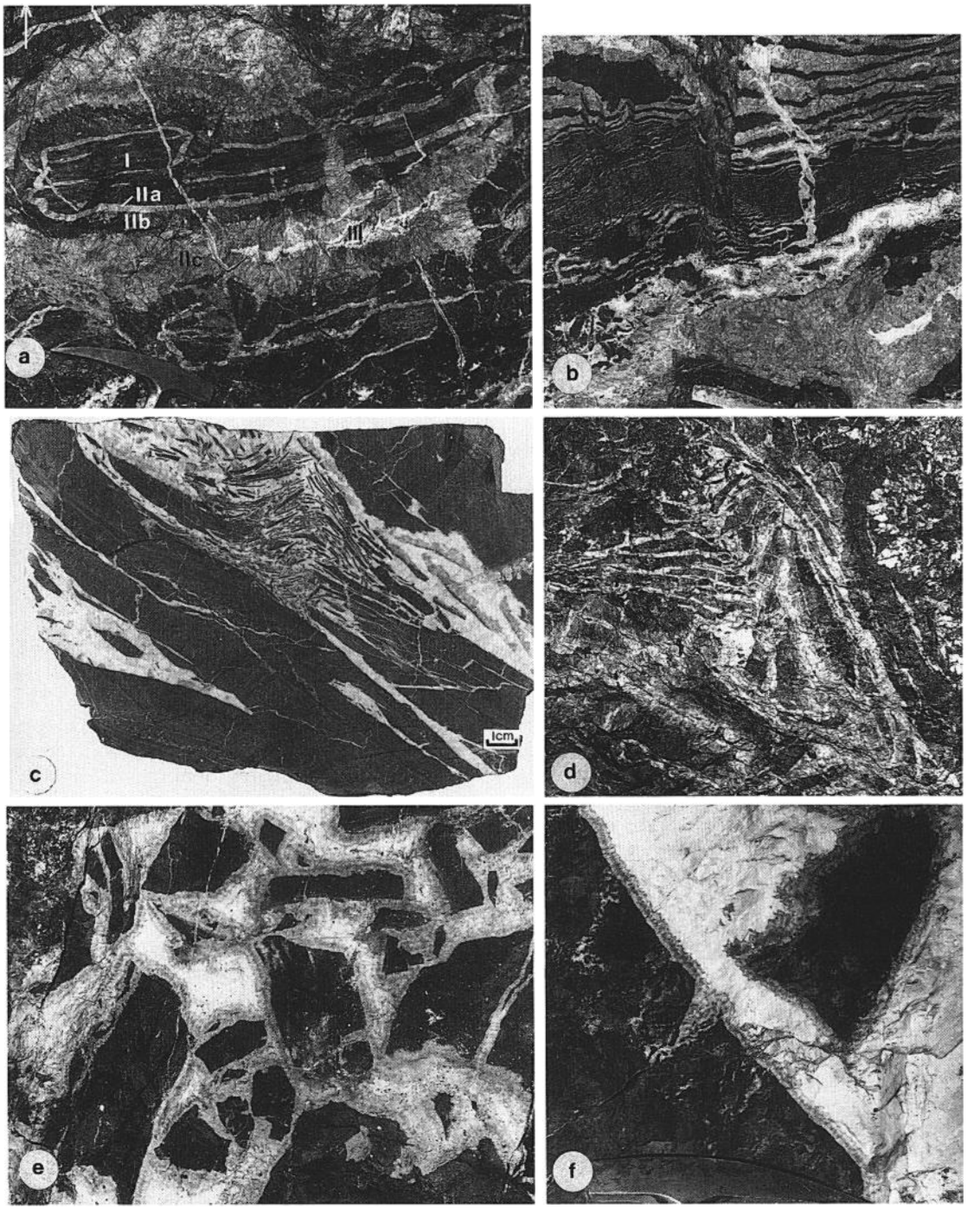

FIG. 14. a. Cockadelike structure with clear dissolution features and repetitions in the paragenetic sequence. I = fine-grained dolomite and sphalerite, IIa = coarsely crystalline dolomite, IIb = brown sphalerite, IIc = sparry dolomite, and III = sparry dolomite with black spots of massive bitumen (1652 N level, crosscut 610E). b. Vein of white sparry dolomite (III) formed during burial diagenesis by deposition from the upward-escaping brine. In San Vicente such veins always point upward. The overpressure regime is clearly indicated by the formation of a stratiform breccia below the layer of dark dolomite (1652 level, gallery 540 N). c. Example of tepeelike structure produced by upward-escaping brines (sampled by P. Levin). The dark broken parts consist of fine-grained dolomite and sphalerite of generation I, the light parts of sparry dolomite (III). d. Similar tepeelike structure (mine wall, 1750 N level, gal 280 S, 70-cm width). e. and f. Hydraulic breccia similar to that shown in b. Subhedral coarsely crystalline dolomite of generation II surrounds the fragments of dark fine-grained dolomite. The matrix is white sparry dolomite and includes a few spots of black bitumen (1652 level, gal 490 N, (e) = 2-m width).

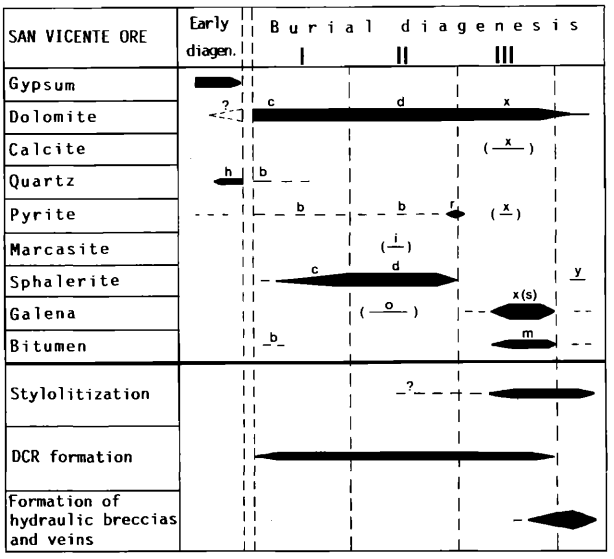

FIG. 15. Paragenetic sequence of the San Vicente ore. The crystallization generations I, II, and III of diagenetic crystallization rhythmites (DCR) are used for reference and also for textures other than diagenetic crystallization rhythmites. Abbreviations: b = very finely disseminated grains, c = medium grained, d = coarsely grained, h = chert, i = inclusions in sphalerite following crystallographic directions, m = massive bitumen, o = only if galena is much more abundant than sphalerite, r = in a thin rim of small euhedral crystals between generations II and III, s = occasionally containing bournonite and other sulfosalts, x = coarsely to very coarsely grained xenomorphic filling, and y = pale yellow. Only occasional occurrences are given in parenthesis.

clusions in sphalerite (Fig. 9f). This sphalerite may contain relatively high Fe values and is sometimes erroneously called marmatite. This pyrite cannot be separated by flotation.

Sphalerite occurs in generations I and II. In the first one it is fine grained and intergrown with dolomite. Sphalerite of generation II is coarsely crystalline, often displaying several subgenerations, the last of which is often pale yellow. Microprobe analyses indicate that generation I sphalerite contains around 1 to 2 percent Fe. Profiles across generation II sphalerite show numerous peaks of high iron content (up to 5 and 6% Fe) separated by low values. The last pale sphalerite is virtually iron free. Colloform sphalerite is seen in places (Fig. 9c).

The greatest amount of galena occurs in generation III (Fig. 10e and f). A small amount is contained as intergranular space fillings in prior generations (Fig. 9e). Galena is usually much less abundant than sphalerite (avg Zn/Pb grades about 12/0.8); however, there are layers in which galena is more abundant than sphalerite. In these layers galena generally crystallizes before the largest part of sphalerite. Calcite, which is occasionally present, crystallizes in generation III.

The paragenetic sequence of the diagenetic crystallization rhythmites can usually be applied to other ore structures. Features indicating dissolution of previously formed ore minerals are observed but are infrequent (Fig. 10c). However, dolomite dissolution is widespread, especially in hydraulic breccias (Fig. 14b, e, and f). The paragenetic position of sphalerite and galena is clearly between the finely to medium crystalline dolomite of generation I and the coarsely crystalline dolomite of generation III. In places, especially in nonrhythmite structures, partial repetitions of the paragenetic sequence are recognized (between dolomite II and sphalerite II, but never with galena; Fig. 9c and d). This recognition and the repeated peaks of Fe in generation II sphalerite denote a minor scale pulsation in the physicochemical conditions of the fluid during ore deposition, but cannot be compared, for instance, with the repetitions of the sequence described for the Viburnum Trend (Hagni, 1983), which indicate sequential mineralization phases. The simple and typical paragenetic sequence of San Vicente is consistent with the series of solubility products of iron, zinc, and lead sulfides (Anderson, 1983; Anderson and Garven, 1987). The absence of important sequence repetitions argues for a single ore-forming event.

The coarsely crystalline dolomite of generation III and the paragenetically slightly later sparry dolomite forming the matrix of the hydraulic breccias and crosscutting veins are essentially postore. The patches of massive bitumen are the latest to be formed, as denoted by their occurrence in geodelike voids in sparry dolomite. Sparry dolomite also predates the regional fault systems affecting the area.

Trace Elements

Lithogeochemistry of the Pucará sequence

A detailed lithogeochemical profile across the sedimentary section at San Vicente has been completed (González, 1987, Fontboté and Gorzawski, 1987). The soluble fraction obtained with a standard HCl and HNO_3 dissolution method was analyzed with atomic absorption spectrophotometry for Fe, Pb, Zn, Cu, Mn, Sr, and Na. Flameless AAS was used for the Ag analyses. In addition, Si, Al, Ca, Mg, Fe, Ti, Sr, K, and Ba were analyzed by XRF (pressed powder tablets). The main results of this investigation can be summarized as follows.

In Table 3 the geometric mean values of the ore-free samples (i.e., those with Zn or Pb values lower than quantile$_{95}$) sorted by lithologic units are presented. Samples which petrographically indicate volcanic influence (i.e., carbonatized volcanic-subvolcanic and tuffaceous rocks) have been grouped separately. In general, the petrographic characteristics are reflected clearly by the lithogeochemistry. Thus, the limestone units—Basal Series, Neptuno Limestone, and Bituminous Silty Limestone—have the

TABLE 3. Major and Trace Element Analyses of Host-Rock Samples

Unit	n°	*n*	SiO_2	Al_2O	CaO	MgO	Fe°	Fe	Ag°	Pb°	Zn°	Cu°	Mn°	Mn	Ti	Sr°	Sr	Na°	K	Ba
AD	1	1	9.1	0.5	29.0	19.3	0.28	0.38	1.00	25	141	20	1,000	1,040	33	50	71	305	840	n.a.
BSL	10	7	8.6	1.0	39.8	1.4	0.11	0.39	0.01	33	20	11	365	228	43	323	556	204	1,786	86
SVD	77	41	0.8	0.1	31.5	20.6	0.17	0.43	<1	32	42	7	1,333	1,333	6	68	84	170	169	20
NL	21	7	2.1	0.3	39.0	11.0	0.12	0.24	<1	30	14	12	112	122	18	81	108	208	678	32
SJD	49	9	1.5	0.2	30.9	20.5	0.33	0.50	0.03	36	9	8	1,542	1,106	8	76	134	311	359	8
BS	64	18	11.9	1.9	34.1	6.7	0.37	0.73	0.04	29	41	14	135	164	85	144	211	261	2,792	66
RS	3	1	26.7	3.1	18.7	0.6	1.25	1.38	<1	19	38	20	585	642	278	129	188	193	2,369	764
Volc	16	12	16.4	8.3	17.5	11.4	1.25	1.93	3.66	32	28	24	718	538	939	57	90	189	1,931	112

SiO_2, Al_2O_3, CaO, MgO, and Fe values in percent, all other values in ppm; AAS analyses of soluble fraction are indicated with an asterisk; all other values are XRF analyses of total sample; additional ICP analyses for Hg from 3 limestone and 11 dolomite samples yield values between 25 and 85 ppb. Abbreviations: AD = Alfonso Dolomite, BSL = Bituminous Silty Limestone, SVD = San Vicente Dolomite, NL = Neptuno Limestone, SJD = San Judas Limestone, BS = Basal Series, RS = Red Sandstone; Volc = carbonatized volcanic, subvolcanic, and tuffaceous rocks; n.a. = not analyzed; *n* = number of samples analyzed.

Analyses performed at Laboratory of the Institute of Mineralogy, Heidelberg

highest CaO contents, whereas the dolomites—San Judas Dolomite, San Vicente Dolomite, and Alfonso Dolomite—have the highest MgO and Mn contents. Sr tends to be enriched in limestones with respect to dolomites. Ti and Fe appear to be diagnostic of volcanic influence. Detrital input is indicated by high K and Sr values coupled with Ti amounts clearly lower than those of volcanic-influenced rocks. The XRF analyses yield higher Sr and Fe values than AAS analyses because significant amounts of Sr are contained in insoluble detrital minerals and because only part of the pyrite was dissolved. In contrast, using both analytical methods, Mn values are similar, indicating that Mn is mainly contained in the carbonate soluble fraction.

The Mn values are higher in the ore-bearing units (1,542 ppm in San Judas Dolomite, 1,333 ppm in San Vicente Dolomite) than in the other carbonate units (135 ppm in the Basal Series, 112 ppm Mn in the Neptuno Limestone, and 365 ppm in the Bituminous Silty Limestone) and are also higher than in other shallow-water dolomitic rocks (e.g., Bencini and Turi, 1974). These high Mn values bear no relation to volcanic activity and are either connected with the dolomitization process or are produced by the influxing basinal brine. The first possibility is favored by low Mn values of the nondolomitized oolitic barrier facies in the upper part of the Neptuno Limestone and high Mn values in the dolomitized portion of the same oolitic barrier facies at the lower part of the San Vicente Dolomite (Fontboté and Gorzawski, 1987).

The mean values for Zn of the group of ore-free samples of the San Vicente Dolomite (42 ppm) and San Judas Dolomite (9 ppm) are not anomalous compared to the rest of the sequence or to dolomitic sequences in other parts of the world. The fact that the zinc values in the whole sequence, including the ore-bearing units, lie within the field of normal sedimentary rocks confirms the visual observation that the ore lenses have very sharp boundaries. Furthermore, the position of Levin (1975) that the whole Pucará is anomalous in Zn cannot be supported.

Trace element content of the ore

Two types of trace element analyses of ores are available. Table 4 contains averages of XRF analyses of selected ore samples (P. Soler, writ. commun., Paris). Table 5 displays analyses on pure sphalerite grains carried out by optical emission spectrography (E. Schroll, writ. commun., Vienna). The low trace element content of the San Vicente ore is typical for Mississippi Valley-type ore deposits and is different from the trace element pattern of the volcanogenic deposits in the central part of the Pucará basin (Soler, 1987).

TABLE 4. Geometric Mean of XRF Analyses of Selected Ore Samples from San Vicente

Manto	*n*	Zn	Pb	Fe	Ag	Cu	Mn	Ge	Sn	Cd	Se
Manto	3	28.4	4.0	1.17	20	367	1,133	116	43	17	1,560
Jesus (rich ores)	3	29.7	4.8	0.58	19	67	900	34	40	33	1,280
Jesus (poor ores)	3	8.7	6.3	0.50	17	150	1,300	79	20	30	860
Ayala	3	34.1	0.7	1.05	52	183	833	38	20	10	2,393

Zn, Pb, and Fe in percent; all other values in ppm; P. Soler, writ. commun., Paris

TABLE 5. Trace Element Analyses on Pure Sphalerite Samples from Ores in the San Vicente Dolomite

Sample	Ag	Co	Cu	Ga	In	Ge	Mn	Mo	Ni	Tl	Va
FSV-3	29.0	7.5	1	8.1	0.33	11	152	1.6	<1	11.0	1.50
FSV-39	23.0	8.8	0	1.3	<0.1	36	52	2.2	<1	7.4	<0.3
FSV-44-IIa	n.a.	n.a.	n.a.	50.0	0.57	62	n.a.	n.a.	n.a.	11.0	n.a.
FSV-44-IIb	n.a.	21.0	73	40.0	0.72	44	285	1.7	3.8	8.0	2.00
FSV-54-I	n.a.	16.0	23	28.0	0.16	49	79	65.0	<1	7.3	0.55
FSV-79	1.5	6.8	1	2.8	0.10	29	95	2.0	4.8	3.7	0.73

All values in ppm; n.a. = not analyzed.
Optical emission spectrography, in part with double arc technique; E. Stroll, writ. commun., Vienna

Isotopic Investigations

This investigation has focused on possible isotopic differences in subsequent generations of carbonates and sulfides in order to characterize the diagenetic evolution of host rock and ore. For this purpose the following main groups of samples from the San Vicente area were carefully selected.[2] Groups B, C, and D correspond to specimens of the ore-bearing San Vicente Dolomite and San Judas Dolomite and Group A also includes host rocks of other lithologic units for comparison: (A) host rocks (seven specimens, seven samples); (B) rhythmites and related textures without ore (nine specimens, 20 samples); (C) ore-bearing rhythmites (seven specimens, 15 samples); and (D) sulfide minerals (sphalerite and galena, seven specimens, 25 samples).

Fifty-three $^{87}Sr/^{86}Sr$ ratios, 41 $\delta^{13}C$ and $\delta^{18}O$ values, and 20 $\delta^{34}S$ values have been determined. A clean separation of the different crystallization generations was obtained by using a modified dental drill and binocular microscope. The strontium isotope ratios were determined at the B.R.G.M. (Orleans, France), and the sulfur isotope analyses were performed by C. W. Field at Oregon State University. The carbon and oxygen isotope analyses were performed by H. Gorzawski at the Max-Planck-Institut für Chemie (Mainz, Germany). The rubidium contents in carbonates were analyzed by AAS by R. Sobott (Preussag-Berkhöpen, Germany), and for comparison, in a few samples, by neutron activation by E. Pernicka (Max-Planck-Institut für Kernphysik, Heidelberg, Germany).

A petrographic description of the specimens analyzed is given in Table 6. The trace element contents are given in Table 7. The selected specimens include the main facies, both ore and nonore bearing.

The geochemical characterization includes AAS analyses for Fe, Mn, Zn, Cu, Pb, Na, Rb, and Sr. For this purpose samples were treated with cold NaCl (1*N*) in order to avoid sulfide dissolution.

[2] For most specimens two or more subsequent crystallization generations were analyzed separately. For this reason the number of analyzed samples in Table 7 largely exceeds that of specimens listed in Table 6.

Dolomite samples from the ore-bearing horizons have a relatively high Mn content, which is consistent with the XRF and AAS analyses of whole-rock samples. In Table 3 note that the sample preparation and some of the analysis methods are different from those in Table 7, therefore a direct comparison of the results is not possible.

The strontium and rubidium contents of generation I lie in the range expected for dolomitic rocks (Wedepohl, 1974). It appears that, with some exceptions, Sr, Rb, and Na contents are generally lower in dolomites of generation I than in corresponding dolomites of generation II.

The other trace elements are not anomalous nor do they display a systematic concentration trend between dolomite generations.

Strontium isotopes

Analytical methods: Strontium for isotope analyses was separated from carbonate and sulfide samples using standard techniques of dissolution and cation exchange chromatography. Strontium isotope ratios were measured on a Finnigan MAT 261 solid source mass spectrometer equipped with a double collector system. During the period of analyses the mean value of 12 analyses of NBS 987 standard was 0.710277 $\pm$ 0.000022 (2 σ_{mean}) for the $^{87}Sr/^{86}Sr$ ratio. The $^{86}Sr/^{88}Sr$ isotope ratios reported in Tables 7 and 8 were normalized to a value of 0.1194 for $^{86}Sr/^{88}Sr$. The $^{87}Sr/^{86}Sr$ ratios were obtained during runs of eight blocks with ten scans each. Error on these ratios is at the 2σ level where $2\sigma_{mean}$ = 2 standard deviation $\sqrt{n}$ blocks. The $^{87}Sr/^{86}Sr$ runs of the sulfide samples were of similar quality and precision to those of carbonate and whole-rock samples (see discussion of results below). Additional analytic details can be found in Gorzawski et al. (1989).

Results and discussion: The results of the $^{87}Sr/^{86}Sr$ analyses on carbonate samples are given in Table 7, those of sphalerite and galena are contained in Table 8, and all results are plotted in Figure 16.

Among the representative host-rock specimens, two limestones and four dolostones from different positions in the stratigraphic sequence were analyzed. The $^{87}Sr/^{86}Sr$ ratios are remarkably similar for all

TABLE 6. Petrographic Description of the Samples Used for Isotopic Studies

Field no.	Anal. no.	Unit	Height[1]	Description
A-052	HGA-118	SVD	0916	DCR, gen. I: medium crystalline do (oolitic packstone with some cryptalgal lamination)
B-054	HGA-117	SVD	0907	Homogenous medium crystalline do (oolitic packstone)
B-064	HGA-120	SVD	0919	Do DCR, medium crystalline do (oolitic grainstone)
D-001	HGA-041	SVD	1035	Medium crystalline do (well-sorted oolitic bioclastic grainstone)
D-009	HGA-049	SVD	1048.2	Do DCR, gen. I: medium crystalline do (oolitic packstone with cryptalgal lamination)
E-037	HGA-042	SVD	0862	Do DCR, medium crystalline do (well-sorted oolitic grainstone) with do veinlets
E-038	HGA-051	SVD	0863	Do DCR, medium crystalline do (oolitic grainstone with cryptalgal lamination) with do veinlets
FSV-007	HGA-059	SVD	0923	Sl-do DCR, fine-grained sl and do (mudstone with cryptalgal lamination)
FSV-009	HGA-122	SVD	0953	Do DCR, finely crystalline do and sl (packstone with algal mats)
FSV-015	HGA-038	BSL	1117	Bituminous silty limestone with fossil fragments (mudstone)
FSV-018	HGA-039	BSL	1145	Bituminous laminated sandy limestone
FSV-038	HGA-044	SVD	0853	Do DCR, layers of finely crystalline do (pellet wackestone with algal lamination) and of medium crystalline do (oolitic packstone)
FSV-039	HGA-046	SVD	0853	Sphalerite with very coarsely crystalline do
FSV-041	HGA-061	SVD	0881	Sl-do DCR, gen. I: sl + medium crystalline do (oolitic grainstone, layers of laminated pellets)
FSV-044	HGA-063	SVD	0923	Sl-do DCR, gen. I: sl-bearing finely crystalline do (pelmicrite?)
FSV-044	HGA-150	SVD	0923	Sl-do DCR, gen. I: sl-bearing finely crystalline do (pelmicrite?)
FSV-052	HGA-053	SJD	0530?	Do DCR, gen. I: medium crystalline do (oolitic grainstone with some cryptalgal lamination)
FSV-052	HGA-054	SJD	0530?	Gen. II: do
FSV-052	HGA-055	SJD	0530?	Gen. III: calcite
FSV-073	HGA-056	SVD	0943	Do DCR, gen. I: medium crystalline do (well-sorted oolitic packstone)
FSV-079	HGA-124	SVD	0953	Do-sl DCR, gen. I: medium crystalline do (packstone to grainstone)
FSV-210-5		SVD	0854	Finely crystalline do (mudstone)
FSV-215	HGA-126	SVD	0923	Sl-do DCR, fine- to medium-grained sl with some do and cryptalgal lamination)
K-043	HGA-040	NL	0755	Do (silty wackstone with lithoclastic fragments, foreslope breccia)
MT-003	HGA-115	RS	−0028	Calcite-cemented sandstone
NEP-12	HGA-187	SJD	0711	Finely crystalline do
T-078	HGA-186	BS	0420.7	Limestone (intramicrite-wackestone)
T-090	HGA-116	SJD	0490	Medium crystalline do (oolitic grainstone)
T-103	HGA-047	SJD	0569	Do DCR, medium crystalline do (bioclastic oolitic grainstone)

[1] Meters above the bottom contact of the carbonate sequence

Abbreviations: DCR = diagenetic crystallization rhythmites, do = dolomite, gen. = generation, sl = sphalerite; BS = Basal Series, BSL = Bituminous Silty Limestone, NL = Neptuno Limestone, RS = Red Sandstone, SJD = San Judas Dolomite, SVD = San Vicente Dolomite

samples (avg = 0.70806, Fig. 16). All of these samples are very slightly enriched in radiogenic strontium compared to the estimated $^{87}Sr/^{86}Sr$ ratio of 0.7075 to 0.7078 for seawater during Upper Triassic and Lower Jurassic times (Burke et al., 1982). Sample MT-003, which was taken from the Red Sandstone at the base of the transgressive sequence, is considerably enriched in radiogenic strontium ($^{87}Sr/^{86}Sr$ = 0.70889).

Material of generation I (generally dark fine-crystalline dolomite) and generation II (white coarse-crystalline dolomite) was analyzed separately for ore-free diagenetic crystallization rhythmites and related textures. The results lie in the same range as those for the host rocks. However, dolomite of generation II is always slightly more radiogenic than dolomite of generation I of the same sample (Fig. 16). In the ore-bearing diagenetic crystallization rhythmites the do-

TABLE 7. Isotope (Sr, C, O) and Trace Element Data of Host Rocks and Gangue Minerals

Samples					Trace elements								Isotopes			
Field no.	Lithologic unit	Manto, locality	Anal. no. (HGA-)	Description	Fe (ppm)	Mn (ppm)	Zn (ppm)	Cu (ppm)	Pb (ppm)	Na (ppm)	Sr (ppm)	Rb (ppm)	$^{87}Sr/^{86}Sr$	2σ	$\delta^{13}C$ (‰, PDB)	$\delta^{18}O$ (‰, PDB)
FSV-018	BSL		39	Bituminous laminated sandy limestone	700	177	181	1.0	15	118	965	5.5	0.70823	0.00005	1.2	−7.0
FSV-015	BSL		38	Bituminous silty limestone	17	369	222	0.3	35	140	1,010	3.1	0.70806	0.00002	1.9	−6.2
FSV-210/5	SVD		185	Finely crystalline dolostone									0.70829	0.00003		
B-054	SVD		117	Medium crystalline dolostone	406	1,236	134		58	321	68	3.1	0.70805	0.00004	[illegible]	−5.9
D-001	SVD		41	Medium crystalline dolostone	900	781	103	0.9	43	240	60	1.7	0.70811	0.00003	1.9	−5.9
Nep-12	SJD		187	Finely crystalline dolostone							74		0.70816	0.00002		
T-090	SJD		116	Medium crystalline dolostone	330	829	9		40	269	46	5.0	0.70780	0.00003	2.1	−6.2
T-078	BS		186	Limestone							105		0.70792	0.00002		
K-043	BS		40	Silty limestone	250	72.5	8	0.6	28	183	125	1.8	0.70817	0.00002	0.7	−6.8
MT-003	RS		115	Calcite-cemented sandstone	7,718	489	37	4.3	46	131	118	8.1	0.70889	0.00002	−4.1	−7.7
FSV-079	SVD	Ayala	124	DCR: black dolomite I + sphalerite									0.70791	0.00004	0.9	−8.1
			125	white dolomite II	27	850	1,690		137	294	231	19.3	0.70803	0.00002	0.1	−9.9
FSV-073	SVD	Ayala	56	DCR: black dolomite I	2,008	1,392	20	0.3	57	25	62	4.8	0.70826	0.00004	1.2	−5.9
			57	white dolomite II	130	1,663	14	11.1	39	260	87	12.9	0.70835	0.00003	0.9	−8.4
			58	white dolomite veinlet									0.70820	0.00006	0.3	−8.9
FSV-009	SVD	Ayala	122	DCR: black dolomite I + sphalerite	43	732	24,000	41.0	100	235	165	0.3	0.70778	0.00004	2.1	−5.8
			123	white dolomite II	163	1,373	2,912	26.0	38	295		184.8	0.70794	0.00001	0.9	−8.4
FSV-215	SVD	3t	126	DCR: black dolomite I + sphalerite	103	543	198,000	1.6	303	162	158	0.3	0.70784	0.00005	1.2	−8.2
			127	white dolomite II	72		503	1,481.0	612	612	202	2.9	0.70786	0.00002	0.6	−9.0
FSV-044	SVD	3t	63	DCR: black dolomite I + sphalerite	2,350	2,202	151	1.0	63	162	67	1.9	0.70781	0.00005	0.9	−6.3
			64	white dolomite II	1,950	1,369	273	1.1	15	230	57	0.5	0.70798	0.00003	0.5	−7.2
FSV-007	SVD	3t	59	DCR: black dolomite I + sphalerite	2,700								0.70786	0.00004	0.5	−6.5
			60	white dolomite II	100								0.70814	0.00003	0.5	−7.1
B-064	SVD	3t	120	DCR: black dolomite I	520	2,194	101	97.1	119	320	56	1.6	0.70807	0.00006	0.8	−6.3
			121	white dolomite II	88	265		20.0	264	742	274	1.8	0.70827	0.00005	−1.1	−10.2
A-052	SVD	3t	118	DCR: black dolomite I + sphalerite	144	1,662	236	96.8	433	1,228	58	0.3	0.70808	0.00005	1.3	−6.3
			119	white dolomite II	137	3,154	64		292	801	137	0.3	0.70818	0.00004	0.8	−6.8
FSV-041	SVD	3p	61	DCR: black dolomite I + sphalerite	4,150	682	250,000	0.4	5,308	113	58	1.1	0.70793	0.00005	0.5	−6.7
			62	white dolomite II	3,032	2,459	1,724	1.3	194	290	93	1.1	0.70799	0.00007	0.4	−8.0
FSV-039	SVD	2	46	White dolomite associated with massive sphalerite	1,650	2,086	13,000	500.0	1,000	235	78	0.8	0.70799	0.00005	0.5	−7.9
FSV-038	SVD	2	44	DCR: black dolomite I	8,750	227	1,000	2.7	540	93	18	0.9	0.70795	0.00004	1.3	−8.0
			45	white dolomite II									0.70798	0.00002	0.7	−8.6
D-009	SVD	SV-south	49	DCR: black dolomite I									0.70801	0.00002	1.1	−6.0
			50	white dolomite II	1,000	2,062	492	4.9	15	243	82	1.8	0.70832	0.00003	0.9	−7.5
E-037	SVD	SV-south	42	DCR: black dolomite I	220	1,071	129	124.0	15	233	63	3.9	0.70824	0.00002	1.6	−6.5
			43	white dolomite II	500	1,450	425	2,770.0	999	3,250	150	10.0	0.70830	0.00004	0.7	−8.3
E-038	SVD	SV-south	51	DCR: black dolomite I	1,982	1,956	47	14.0	64	212	47	0.3	0.70815	0.00005	1.1	−6.9
			52	white dolomite II	51	1,216	166	21.2	83	300	119	5.4	0.70819	0.00005	1.0	−8.6
FSV-052	SJD	Chilpes	53	DCR: black dolomite I	65	64		1.0	40	255	157	2.0	0.70802	0.00003	1.2	−6.6
			54	gray dolomite II	2,150	2,044	25	1.3	25	258	93	3.7	0.70822	0.00003	1.0	−6.9
			55	white calcite III	50	530	670	1.2	15	138	880	2.5	0.70827	0.00006	−1.7	−10.3
			53b	insoluble residue (in generation 1)									0.70815	0.00002		
T-103	SJD	Tunnel	47	DCR: black dolomite I	710	1,704	43	81.2	160	481	91	3.2	0.70792	0.00004	1.4	−6.2
		Uncush	48	white dolomite II	223	513		1,509.0	669	1,228	513	5.5	0.70817	0.00003	1.1	−7.7

See Table 6 for abbreviations

TABLE 8. Results of S and Sr Isotope Determinations of Sulfide Samples from San Vicente

Field no.	Lithologic unit	Manto	Anal. no. (HGA-)	Description	$\delta^{34}S$ (‰, CDT)	$^{87}Sr/^{86}Sr$	2 σ
FSV-039	SVD	2	92	Massive sphalerite	12.1		
			149	Massive sphalerite	12.2	0.70838	0.00022
			153	Galena	6.8	0.70810	0.00004
FSV-041	SVD	3p	78	DCR: sphalerite I	13.0		
			79	DCR: sphalerite II	12.8		
			80	DCR: galena	6.9		
FSV-007	SVD	3t	75	DCR: sphalerite I	10.4		
			76	DCR: sphalerite IIa	9.7		
			77	DCR: sphalerite IIb	9.4		
FSV-044	SVD	3t	81	Sphalerite	10.1		
			82	Sphalerite	11.0		
			83	Sphalerite	11.0		
			84	Sphalerite	9.9		
			85	Sphalerite	11.5		
			86	Sphalerite	10.8		
			87	Sphalerite	10.0		
			88	Sphalerite	10.8		
			89	Sphalerite	10.2		
			150	DCR: sphalerite I		0.70816	0.00008
			151	DCR: sphalerite II		0.70873	0.00003
FSV-215	SVD	3t	154	Galena		0.70798	0.00003
FSV-009	SVD	Ayala	122	DCR: sphalerite I		0.70788	0.00002
			148	DCR: sphalerite II		0.70803	0.00002
FSV-079	SVD	Ayala	124	DCR: sphalerite I	10.6	0.70796	0.00003
			152	DCR: sphalerite II	9.9	0.70809	0.00001

See Table 6 for abbreviations

lomite of generation II is generally also slightly more radiogenic than that of generation I (Fig. 16).

The last set of samples comprises sulfide minerals (Table 8). In selected specimens different sulfide generations were separated. The analytic results show that $^{87}Sr/^{86}Sr$ ratios for sulfides are generally higher than for carbonates from the same specimen. According to their position in the crystallization sequence, the later sulfides are slightly but significantly enriched in radiogenic ^{87}Sr compared to the earlier dolomite or sulfide generations. For this discussion, it is irrelevant if the measured strontium ratios correspond ac-

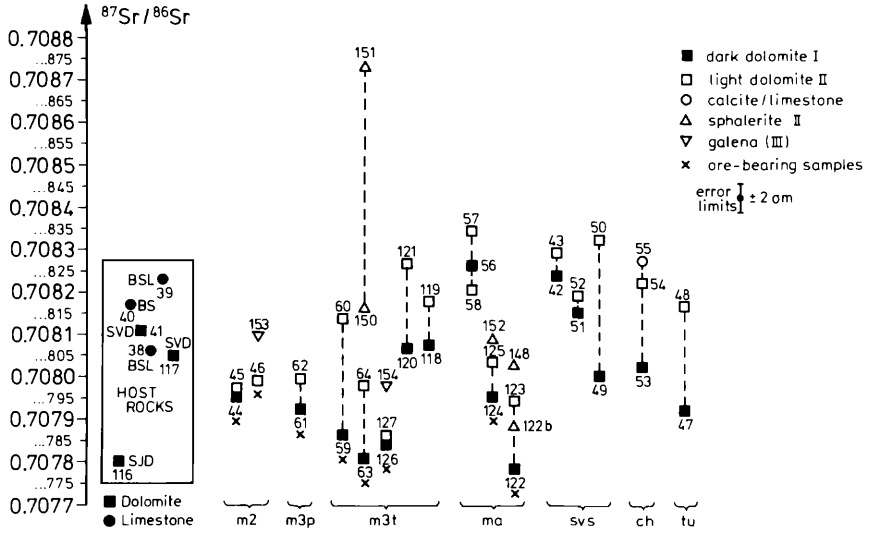

FIG. 16. Results of strontium isotope analyses. Numbers correspond to numbers in Tables 7 and 8. m2 = manto 2; m3p = manto 3 piso; 3t = manto 3 techo; ma = manto Ayala; svs = San Vicente south; ch = Chilpes; tu = Uncush tunnel.

tually to Sr bound in the sulfide lattice or to very minute fluid or carbonate inclusions. The point is that these data reflect the $^{87}Sr/^{86}Sr$ ratio during sulfide precipitation. A possible problem of the $^{87}Sr/^{86}Sr$ ratios in sulfides is that as the strontium content in sulfides is very low (less than 1 ppm), the influence of the Sr blank is not negligible, and any Sr contamination would lead to an increase of the ^{87}Sr proportion measured.

Summarizing the results: (1) the values for the four groups studied lie in a relatively narrow range of $^{87}Sr/^{86}Sr$ ratios, between 0.70778 and 0.70835; (2) the lowest value of 0.70778 lies close to the range of 0.7075 to 0.7078 presented by Burke et al. (1982) for Upper Triassic to Lower Jurassic seawater; and (3) despite the narrow variation range of the strontium isotope values, there are systematic differences in the strontium isotope ratios. The dolomites (and sulfides) of generation I are always less radiogenic than the corresponding carbonates (and sulfides) of the later generations II or III. Laboratory leaching of silicates (compare Banner et al., 1988) can be excluded as the factor responsible for this trend because generation I, having some insoluble residues, is always less radiogenic than generations II or III, which are virtually free of insoluble residues. An additional test was carried out by analyzing the $^{87}Sr/^{86}Sr$ ratio of the insoluble residue in one sample (FSV-052, generation I). The strontium isotope ratio thus obtained is slightly higher than that of the coexisting dolomite I, but still lower than the isotopic ratio of the carbonate generations II and III of the same specimen.

Theoretically one might expect a dependence of the $^{87}Sr/^{86}Sr$ ratios on the Rb content of the carbonates. This is only possible if the Rb/Sr ratio is high enough. The data presented here indicate that the ratios are very low (Table 7) and therefore this influence is negligible. Clauer (1976) and Moore (1985) obtained similar results.

There are only a few other published studies in which strontium isotope ratios of different diagenetic crystallization generations were distinguished. In most cases where this distinction was made, the strontium ratios increase with the crystallization sequence (Kessen et al., 1981; Grant and Miranda, 1983; Lange et al., 1983; Moore, 1985; Woronick and Land, 1985; Kesler et al., 1988; Gorzawski et al.; 1989). It is therefore concluded that the trend observed in this study corresponds to the rule that the minerals formed at the end of a diagenetic crystallization sequence are, in general, more radiogenic than those formed at the beginning.

The isotopic composition of the strontium in San Vicente is dominated by strontium with seawater composition contained in carbonate rocks and released by the dolomite replacement of calcite and sulfates. Therefore the introduction of a more radiogenic brine is required to explain the shift toward more radiogenic values late in the paragenesis. In situ element exchange between silicate and carbonate phases during burial diagenesis (as suggested by Veizer and Compston, 1974) can play only a very subordinate role because of the extremely low content of detrital particles in the San Vicente Dolomite. The measured strontium isotope ratios are the result of mixing and equilibration between the brine—relatively enriched in radiogenic strontium—and the carbonate host rocks which have strontium isotope compositions very close to Upper Triassic to Lower Jurassic seawater. The brine/host-rock ratio determining the strontium isotope ratio of the fluid from which the coarse crystalline dolomites and sulfides of the late generations precipitated increases progressively from generation I, where primary sedimentary structures can still be recognized. This is the main explanation for the higher proportion of radiogenic strontium in late generations.

The exact strontium isotope composition of the influxing brine is not known. Examination of the data in Figure 16 suggests that the $^{87}Sr/^{86}Sr$ ratio of the brine should lie close to or above 0.7084 because 52 of the 53 ratios are lower than this value. The only exception (sphalerite, sample 151 with a value of 0.70873) has, however, some analytic uncertainty, as the possibility of blank contamination cannot be ruled out.

A basinal brine that circulated through detrital sediments could be the source of the relatively radiogenic strontium. Numerous investigations show that recent basinal brines have a wide range of strontium isotope compositions and that there is evidence indicating that the brines became enriched in ^{87}Sr by exchange reactions with detrital host sediments or with basement rocks (Chaudhuri, 1978; Sunwall and Pushkar, 1979; Starinsky et al., 1983; Walter et al., 1987). Several reactions can release radiogenic strontium from detrital minerals to interstitial solutions, among the most important are feldspar alteration and illite formation (Stueber et al., 1984; Gieskes et al., 1986; Chaudhuri et al., 1987). Russell (1985) shows that the increase in the $^{87}Sr/^{86}Sr$ ratios in brines in southeastern Mississippi can be correlated with burial to a depth of 3,000 m and explains this by progressive alteration of rubidium-bearing detrital minerals.

The trend to ^{87}Sr-enriched compositions in later crystallization generations is also observed in other Mississippi Valley-type ore deposits (Kessen et al., 1981; Lange et al., 1983; Medford et al., 1983; Gorzawski et al., 1989). However, the absolute increase in those of the strontium ratios at San Vicente is much lower than, for instance, in the Viburnum Trend and Pine Point (Fig. 17). The small increase of the $^{87}Sr/^{86}Sr$ ratios at San Vicente could indicate a relatively low stage of maturity of the basin at the time of brine

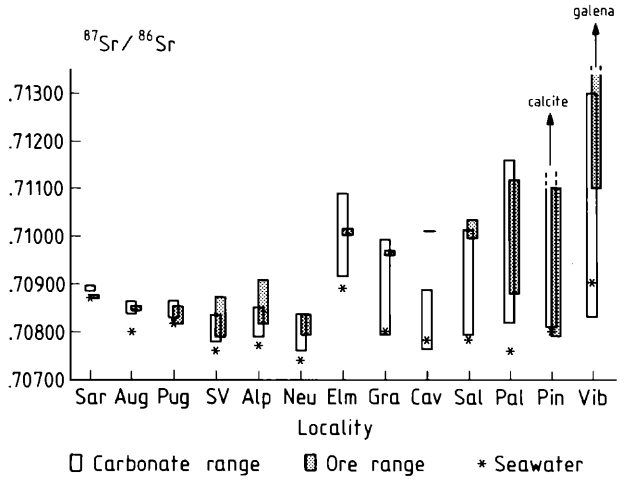

FIG. 17. Variation ranges of strontium isotope compositions of San Vicente compared to data for other Mississippi Valley-type districts. Sar = Caneli Aquas, Sardinia, Italy (Gorzawski et al., 1989); Aug = Auglaize quarry, Ohio; Pug = Pugh quarry, Ohio; SV = San Vicente (present study); Alp = Alpujarrides, southern Spain; Neu = Neuquén, Argentina; Elm = Elmwood, Tennessee; Gra = Gratz - Lockport, Kentucky; Cav = Cave-in-Rock, Kentucky; Sal = Salem, Kentucky; Pal = Croix des Palières, southern France; Pin = Pine Point, Canada (Medford et al., 1983); Vib = Viburnam Trend, Missouri (Large et al., 1983). Data for Ohio and Kentucky are from Kessen et al. (1981). The estimated composition of contemporaneous seawater for each deposit is indicated with a star (seawater according to data from Veizer and Compston, 1974; and Burke et al., 1982).

migration and ore formation as discussed by Gorzawski et al. (1989).

In San Vicente a basinal brine could have incorporated radiogenic strontium from several sources of detrital minerals. These are the Mitu Group, the Red Sandstone underlying the carbonate sequence, and the Lower Sarayaquillo Formation which contains clastic material eroded from the Brazilian Shield. The two last possibilities are favored because the lead isotope evidence (see below) rules out the Mitu Group as a significant source and indicates that the brine-leached detrital material eroded from an old upper crust.

In addition there is a facies dependence of the strontium isotopes. Samples from lagoonal or tidal flat facies have generally lower strontium isotope ratios than samples from the oolitic barrier (Fig. 18). This was previously interpreted in terms of different mixing ratios between the radiogenic intraformational fluid and ocean water in relatively early stages of diagenesis, depending on the facies position (Fontboté and Gorzawski, 1988). However, this hypothesis must be rejected because the minerals appear to have crystallized under burial exceeding 2 km. The reason for the facies dependence of the strontium isotope ratios should therefore be sought in the lithologic characteristics of the implicated facies. A theoretical possibility would be that the more radiogenic samples contain more Rb-bearing clay minerals. This idea can be discarded because the oolitic grainstones of the barrier facies, characterized by more radiogenic values, are virtually free of clay minerals. A better explanation is that the facies dependence of the strontium isotope values is due to a higher brine/host-rock ratio in the more porous oolitic grainstones of the barrier facies than in the less porous fine-grained facies in the lagoon and tidal flat.

Oxygen and carbon isotopes

Analytical methods: The carbonate samples used for strontium isotope studies were also analyzed for carbon and oxygen isotopes. Carbon dioxide was evolved from powdered samples by reaction with 100 percent phosphoric acid at 25°C according to the procedure described by McCrea (1950) and analyzed on a modified Varian MAT CH5 mass spectrometer equipped with a double inlet and two collector systems. Standard correction procedures were employed (Craig, 1957), but no correction was applied for the possible differences of the fractionation factor between phosphoric acid and calcite or dolomite (Sharma and Clayton, 1965). The results are expressed in per mil difference from the PDB international standard. The reproducibility of the results is ±0.2 per mil for $\delta^{13}C$ and ±0.3 per mil for $\delta^{18}O$.

Results and discussion: Results of oxygen and carbon isotope analyses for San Vicente are given in Table 7 and Figures 19, 20, and 21.

The $\delta^{18}O$ values of host rocks plot very close in a range of −5.5 to −7.8 (Fig. 19). This corresponds to reported values for normal Lower Jurassic carbonates (Veizer and Hoefs, 1976). Dolomite samples of generation I are in the same range as the host rocks.

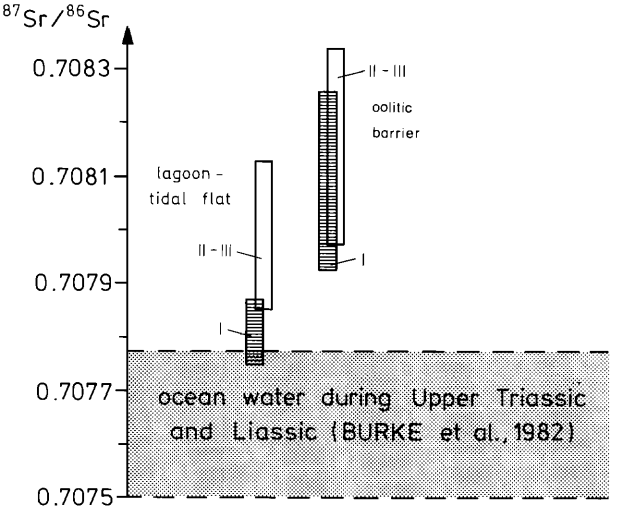

FIG. 18. Variation ranges of the strontium isotope ratios according to the facies position of the analyzed samples. I, II, and III are the crystallization generations observed in diagenetic crystallization rhythmites.

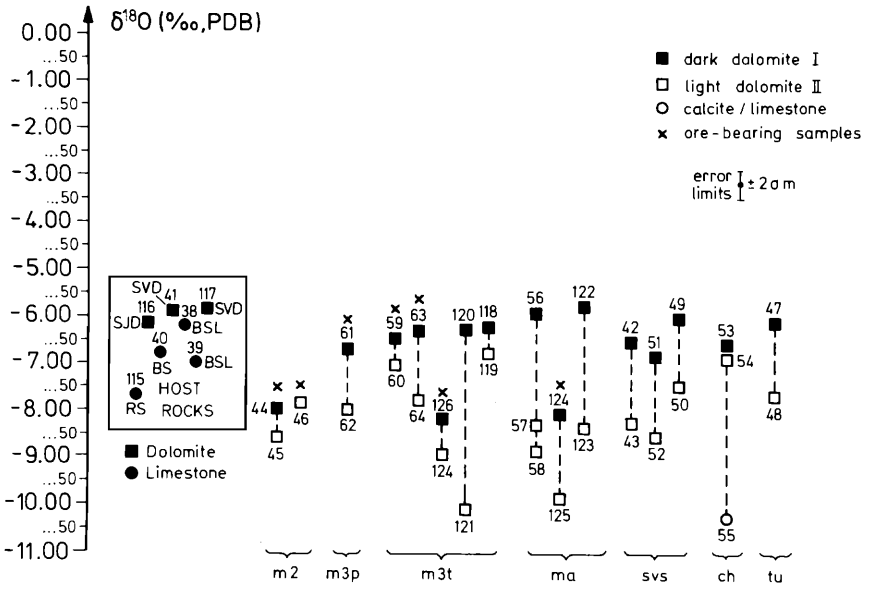

FIG. 19. Results of oxygen isotope analyses. Numbers correspond to numbers in Table 7. m2 = manto 2; m3p = manto 3 piso; m3t = manto 3 techo; ma = manto Ayala; svs = San Vicente south; ch = Chilpes; tu = Uncush tunnel.

However, with advancing diagenesis there are consistent differences in the oxygen isotope composition. The dolomite of generation II is always slightly depleted in $\delta^{18}O$ compared to generation I of the same sample.

The diagram for the carbon isotope compositions (Fig. 20) shows a similar pattern. Host rocks yield $\delta^{13}C$ values which vary within a narrow range from 2.2 to 0.5, which again is a typical range for Lower Jurassic marine carbonates (Veizer and Hoefs, 1976). The other samples lie in the same range of $\delta^{13}C$ values. Again, the light-colored generation II dolomite is always slightly depleted in ^{13}C relative to the corresponding dolomite I.

In summary: (1) the carbonates from San Vicente are remarkably homogeneous in their carbon and oxygen isotope compositions; (2) although the variation ranges in the isotopic compositions of carbon and oxygen are relatively small, a significant evolution toward a lighter isotopic composition with advancing

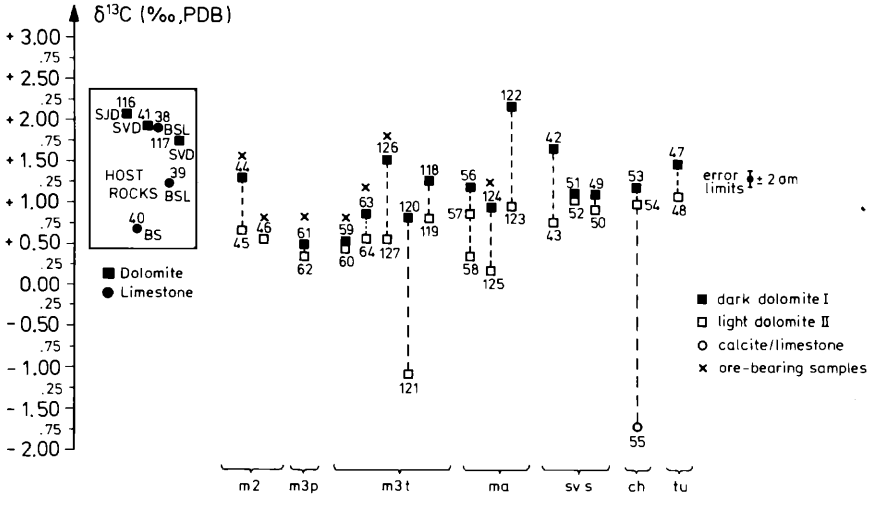

FIG. 20. Results of carbon isotope analyses. Numbers correspond to numbers in Table 7. m2 = manto 2; m3p = manto 3 piso; m3t = manto 3 techo; ma = manto Ayala; svs = San Vicente south; ch = Chilpes; tu = Uncush tunnel.

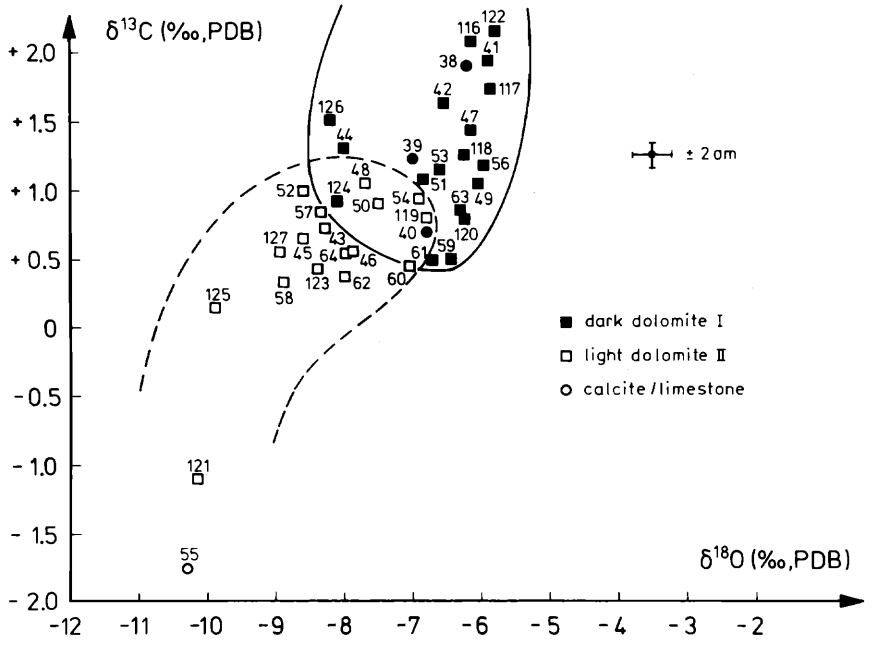

FIG. 21. Plot $^{18}O/^{16}O$ versus $^{13}C/^{12}C$.

diagenesis is observed; and (3) this evolution is independent of the presence or absence of ore minerals.

Several sedimentologic studies have recently been published dealing with stable isotope variations in carbonate cements and rocks. They establish that small isotopic changes of oxygen and/or carbon in sedimentary carbonates are common features that often provide useful tools to characterize the diagenetic evolution. During progressive diagenesis a decrease in $\delta^{18}O$ in subsequent diagenetic stages seems to be typical (Dickson and Coleman, 1980; Meyers and Lohmann, 1985; Moore, 1985, Woronick and Land, 1985). These and other results obtained in nonore-bearing carbonate sequences are similar to the pattern observed at San Vicente.

The narrow range of oxygen isotope variation is indicative of a lack of in situ meteoric influence during the crystallization of generations I and II (Allan and Matthews, 1982). However, a meteoric component in the incoming brine is not incompatible with the oxygen isotope results. Inasmuch as a burial environment is assumed, changing temperature conditions could become an important factor for isotope fractionation processes. Crystallization of the different carbonate generations at progressively increasing temperatures would result in a progressive depletion of ^{18}O in the crystallizing carbonate (Dickson and Coleman, 1980), although exact data for the equilibrium isotope fractionation between dolomite and water at low temperatures are not available.

Two facts indicate that temperature fractionation alone cannot explain the stable isotope evolution in the different carbonate generations. The isotopic differences between subsequent generations should be similar within the deposit because the temperature increase should be roughly the same for all samples in a comparable paragenetic position. This, however, is not the case (compare Figs. 19 and 20). Also the differences in $\delta^{18}O$ and $\delta^{13}C$ of the different dolomite generations of single samples do not correlate (Fig. 21) as well as would be expected if the isotopic differences depended only on fractionation coefficients.

A mixing model similar to that discussed for the strontium isotope compositions is necessary to explain the carbon and oxygen isotope compositions of the carbonates. The carbon and oxygen isotope ratios of the precipitated carbonates probably changed for several reasons: (1) the circulating brine had a different carbon and oxygen isotope composition from the seawater that precipitated the original carbonates (generation I), (2) variable fluid/host rock mixing ratios, and (3) temperature increases. Even an influxing brine enriched in ^{18}O would be possible, provided the temperature of crystallization was high enough. However, extremely high temperatures are considered unrealistic because the normal temperature for a burial depth of about 2 to 3 km is estimated on the basis of sulfur isotope geothermometry and fluid inclusions. In addition, depleted oxygen isotope values appear to be a typical feature of burial diagenesis (Land, 1985). The influence of temperature on the carbon isotope composition of dolomite being precipitated from a fluid is not well known. A possible additional carbon source is light carbon of organic

matter dispersed in the host rock or from other parts of the basin. The oxidation of organic matter, with $\delta^{13}C_{organic}$ = about −25 per mil/PDB, releases light carbon, which can contribute to the total HCO source for carbonate precipitation. The minor change observed for the $\delta^{13}C$ values rules out in situ organic carbon as a major source for the carbonate carbon of generations II or III, since greater variations with respect to generation I and relative to the host rocks would be expected (Irwin et al., 1977).

Progressive in situ depletion of the heavier isotopic components during crystallization of the different generations could play a certain role in the last phases of crystallization in carbonate reservoirs. If the system eventually became closed to fluid migration, preferential concentration of the heavier isotope in earlier formed carbonates would deplete the ^{13}C of the residual fluid, which is the source for the later generations (Kelts and McKenzie, 1982; Hannah and Stein, 1984).

In summary, the carbon isotope data indicate a fluid changing slightly but consistently during ore formation. The oxygen and carbon isotope composition of the fluid was mainly controlled by the introduction of a brine probably with a different isotopic composition and by mixing ratios between this fluid and the host rock. A possible subordinate contribution of organically derived carbon, and the influence of slightly increasing temperatures, is also consistent with the carbon and oxygen isotope results.

Sulfur isotopes

Analytical methods: Analyses reported in this study are discussed in Gorzawski et al. (1990) and are carried out on 20 individual sulfide concentrates that were extracted from five samples. The sulfide sulfur in each concentrate was converted to SO_2 gas for mass spectrometric analysis of the sulfur isotope ratio according to the method described by Ohmoto and Rye (1979). The sulfur isotope data are given in convential $\delta^{34}S$ values, representing the deviation of the sample in parts per thousand (‰) relative to the Canyon Diablo meteorite standard (CDT). Analytic precision is calculated to be better than ±0.2 per mil. The data are listed in Table 8 and are graphically displayed in Figure 22 which also includes the earlier results of Nielsen (in Schulz, 1971) for comparison.

Results indicate that sulfides from San Vicente are isotopically remarkably homogeneous, are significantly enriched in ^{34}S, and exhibit a consistent though weak isotopic trend with paragenesis. Many of these features are characteristic of other Mississippi Valley-type deposits as summarized by Heyl et al. (1974) and Ohmoto and Rye (1979). The $\delta^{34}S$ values of 18 sphalerite samples range narrowly from 9.4 to 13.0, and those of two galena samples from 6.8 to 6.9. All sulfides are enriched in ^{34}S relative to those of presumed magmatic or magmatic hydrothermal origin (0 ± 3‰), which implies an isotopically heavy source of sulfur derived from sulfate in oceanic and/or connate waters, or from marine evaporites.

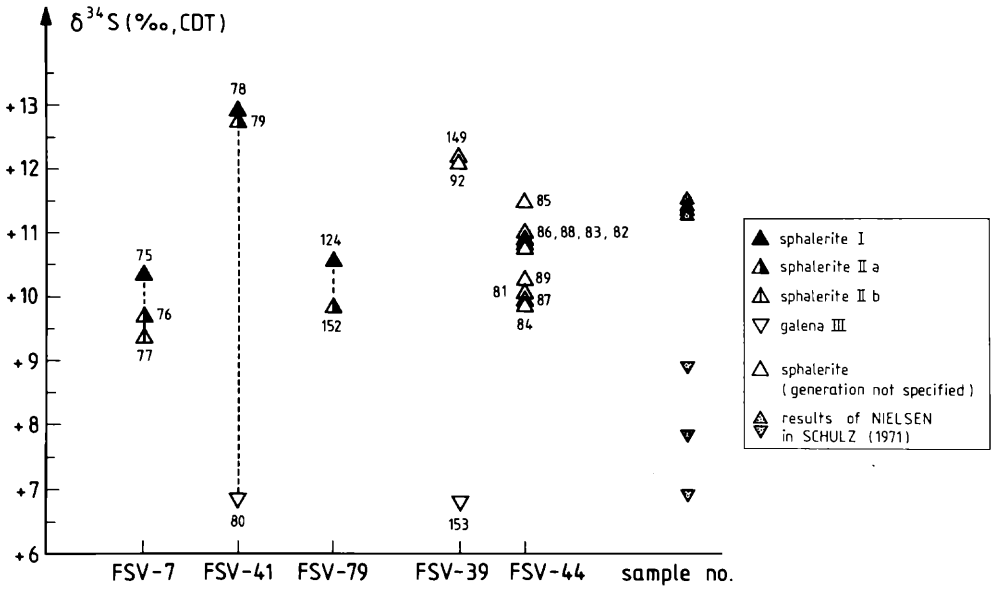

FIG. 22. Results of the sulfur isotope analyses (from Gorzawski et al., 1990). Numbers correspond to numbers in Table 8.

The isotopic homogeneity of sulfur in sulfides from San Vicente was previously noted by Schulz (1971), who attributed this to a later homogenization process. However, such a process is considered unlikely based on the results of the present investigation and because of the absence of a metamorphic imprint on host rocks and ores at San Vicente. Our results demonstrate the existence of small systematic isotopic differences between consecutive sphalerite generations. In the three specimens where a proper separation was possible the first sphalerite generation shows higher $\delta^{34}S$ values than the later sphalerite generations (II, III). This trend toward lighter $\delta^{34}S$ values during sulfide formation may reflect fractionation processes and mass-balance effects related to changing physicochemical parameters of the system. Decreasing fractionation between ZnS and H_2S with increasing temperature during progressing diagenesis would be one possible explanation, but unrealistically high temperature increases would be required between consecutive sphalerite generations.

Clear constraints can be set regarding the source of sulfur for the sulfides at San Vicente. According to Claypool et al. (1980) the sulfur isotope composition of marine sulfate ranged from about 12 to 18 throughout the Middle Triassic to Lower Jurassic. In addition, Field et al. (1983) reported $\delta^{34}S$ values of 13.1 and 13.8 for evaporitic anhydrite within the Morococha district in the western part of the Pucará basin.

Abundant petrographic data show that in San Vicente sulfate minerals have been replaced by carbonates. In the temperature range of formation of Mississippi Valley-type deposits the replacement of sulfate by carbonate in the absence of other reactions can be taken as evidence for sulfate reduction (Anderson and Garven, 1987). This is because the hydrogen ions generated by sulfate replacement would inhibit the precipitation of carbonate phases in the absence of sulfate reduction or other reactions such as silicate alteration.

The isotopically heavy and uniform $\delta^{34}S$ values of the sphalerites are inconsistent with a biogenic mechanism for the reduction of sulfate in place. Also the generation of H_2S by thermal degradation of organic sulfur-bearing hydrocarbons is not considered to produce reduced sulfur with the required sulfur isotope composition for the fixation of metals at San Vicente (Gorzawski et al., 1990).

Abiogenic reduction of sulfate by reactions with organic carbon, ferrous iron, or H_2 may generate H_2S that is but slightly to moderately fractionated relative to the source of sulfur. Orr (1974, 1977) proposed that hydrocarbons in combination with H_2S may reduce sulfates at temperatures as low as 80°C. Similarly MacQueen and Powell (1984) and Powell and MacQueen (1984) have suggested that thermochemical reduction of sulfate by bitumen may have formed the sulfide ores of the Pine Point deposit (Canada) at temperatures of about 100°C.

Because of the lack of successful laboratory experiments in reducing abiogenically sulfate below 250°C there is some doubt about the significance of abiogenic sulfate reduction as an ore-forming process in Mississippi Valley-type deposits (Trudinger et al., 1985). However, Orr (1974) and Powell and MacQueen (1984) have suggested that extrapolation of the kinetic data indicates the feasibility of this process at temperatures as low as 80° to 120°C in geologic systems. Moreover, the likelihood and speed of this abiogenic reduction may be enhanced by the presence of partly oxidized intermediate sulfur species (Spirakis, 1986).

The consistency of the $\delta^{34}S$ values could alternatively be indicative for H_2S production and homogenization elsewhere and migration of this homogeneous H_2S to the San Vicente site. However, as discussed later, facies constraints make this possibility quite unlikely. Thus, the sulfur isotope distributions in sulfides from San Vicente are interpreted as a result of H_2S production by abiogenic reduction of sulfates present in the host carbonate.

Assuming equilibrium between the sulfides of generations II and III, isotopic temperatures of 75° and 92°C have been calculated for two sphalerite-galena pairs (FSV-41, FSV-39) using the fractionation equations given by Ohmoto and Rye (1979). This temperature range is consistent with that indicated by scarce fluid inclusion data (see below) and partly overlaps the temperature range at which the thermochemical reduction of sulfate is considered to be possible.

Fluid Inclusions and Organic Matter

Fluid inclusions in the San Vicente ore are characterized by their extremely small size. The Japan International Cooperation Agency (1976) reports from attempts to study three samples from the main ore horizon in San Vicente, one from Siete Jeringas, and one from Uncush Sur. Most of the inclusions are less than 1 to 2 μ with very high filling ratios—about 95 percent. The inclusions are so minute that only a few dolomite samples were actually measured, giving a homogenization temperature range from 70° to 140°C. No freezing temperatures could be determined. In the present investigation the very small size of the fluid inclusions in sphalerite prevented the gathering of more precise data.

Studies on organic matter include reflectivity measurements and Rock-Eval analyses. Organic material in the bituminous limestone consists mainly of bituminous substances showing high reflectance ($R_{max,oil}$ = 4.6%). Rock-Eval analyses of bituminous organic matter from various wall rocks also indicate a high

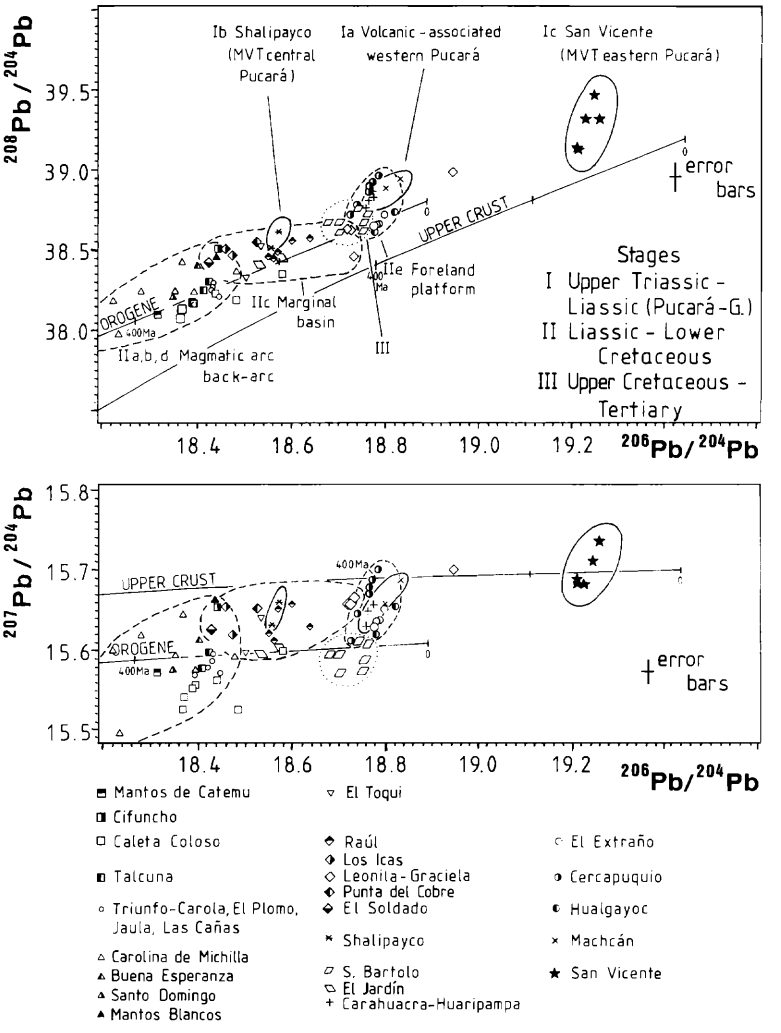

FIG. 23. Lead isotope ratios from San Vicente compared to other strata-bound ore deposits in the Andes. The field of the Pucará ratios is decidedly more radiogenic than fields for the other groups of strata-bound ore deposits hosted by Pucará rocks (see also Fig. 1) and for other Andean strata-bound deposits (from Fontboté et al., 1990a). Data from Mukasa (1984); Flint (1986); Flint et al. (1986); Puig (1988); Macfarlane (1989); Fontboté et al. (1990a and b); and Gunnesch et al. (1990).

maturity, largely beyond the stage of oil and gas generation. This high evolution stage is interpreted to have been attained in postore stages when burial reached depths over 5,000 m.

Lead Isotope Investigations

Gunnesch et al. (1990) report lead isotope analyses of several galena samples from the San Vicente mine. As seen in Figure 23, where these analyses are compared to lead isotope ratios from Andean strata-bound ore deposits located in other paleogeographic and geotectonic positions, the San Vicente ores are by far the most radiogenic. They are also different from other Pucará-hosted ore deposits, including volcanic-associated deposits at the Domo de Yauli, at Huaripampa and Carahuacra, and the Mississippi Valley-type deposit Shalipayco, which is located at the base of the Pucará Group near the contact with volcaniclastic rocks of the Mitu Group. The highly radiogenic values of San Vicente can be compared to the still more radiogenic J-lead range in the Mississippi Valley district which is characterized by negative or future model ages. This is typical of upper crustal lead in cratonic regions and of many Mississippi Valley deposits in this environment (Doe and Zartman, 1979). These results are therefore wholly consistent with the paleogeographic position of San Vicente at the western margin of the Brazilian Shield. An important part of the lead in San Vicente could have been derived from old upper crust from the Brazilian Shield (Fontboté et al., 1990b). Geologic evidence, including the basin geometry, makes leaching of clastic rocks

eroded from the Brazilian Shield (Lower Sarayaquillo Formation and equivalents like the Red Sandstone at San Vicente) more probable than direct leaching of crystalline rocks of the Precambrian basement. Mitu Group volcanic and volcaniclastic rocks cannot be a main source because much less radiogenic values, in the range of those found in Shalipayco (Fig. 23), should be expected (Fontboté et al., 1990b).

Gunnesch et al. (1990) have also measured the lead isotope composition of host-rock carbonates in the San Vicente sequence without directly associated orebodies. The lead in these carbonates is significantly less radiogenic than the lead in the ore samples, thus indicating different sources. This observation is consistent with the strontium isotope results which reveal an input from brines that were slightly enriched in radiogenic strontium. The San Vicente lead isotope data taken as a group are much more radiogenic than data for other Andean ore deposits (Fig. 23), but within the group they display a significant scatter. This could point to mixing between a Precambrian radiogenic component and another less radiogenic component, as suggested for the Viburnum Trend by Crocetti et al. (1988).

Conclusions

The diagenetic evolution of the San Vicente ore deposit has been traced combining petrographic and isotopic data. Significant isotopic trends were found and physicochemical constraints concerning the genesis of the deposit were derived.

The strontium isotope determinations of host rock and gangue and ore minerals yield $^{87}Sr/^{86}Sr$ ratios which all lie in a very narrow range (between 0.7077 and 0.7084), slightly higher than the estimated strontium isotope composition of seawater during Late Triassic-Lower Jurassic times. In detail, small but significant isotopic trends are recognized and reflect the evolution of the fluids during the formation of the ore deposit. The late crystallization generations are always slightly enriched in radiogenic strontium compared to the first ones. These results reveal the introduction of a basinal brine relatively enriched in radiogenic strontium, probably due to circulation through Rb-bearing detrital rocks. Equilibration at different mixing ratios between strontium contained in the brine and in the host rock can explain the observed patterns. For the last generations the brine/rock ratio was higher and therefore the values are also more radiogenic. In addition, the strontium isotope composition of the basinal brine evolves with time toward more radiogenic ratios as a consequence of an increasing exchange reaction with Rb-bearing phases. Combined evidence of strontium and lead isotope determinations suggests that clastic rocks eroded from the Precambrian upper crust of the Brazilian Shield (Lower Sarayaquillo Formation and equivalents like the Red Sandstone at San Vicente) are the most probable source for the radiogenic strontium.

The association of the orebodies with definite algal mat peritidal facies characterized by the presence of molds of sulfates and abundant organic matter is the main evidence supporting a genetic model based on the existence of two separate reservoirs for sulfur and the metals, as proposed by Beales (1967) for Pine Point, rather than a model based on a single brine which introduces sulfur and the cations (e.g., Barnes, 1983; Rickard, 1983; Sverjensky, 1984). This is also consistent with the sulfur isotope values which are relatively heavy and homogeneous and coincide with those of sulfate in other parts of the Pucará basin. These values exclude both magmatic sulfur and in situ biogenic reduction of sulfate as sources for sulfide formation. Abiogenic reduction of sulfate with no or only minor fractionation can better explain the data. The association with evaporite-bearing facies suggests that the sulfur was reduced from the anhydrite and gypsum present in and in the vicinity of the ore deposition site, as evidenced by abundant sulfate pseudomorphs. Considering the evaporite-bearing facies at the district scale and the fact that sulfate pseudomorphs are also abundant in nonore-bearing parts of the dolomite units, the available amount of sulfur should have been sufficient for ore deposition. Although abiogenic reduction of sulfates has not been achieved experimentally in the temperature range indicated by the sulfur isotope geothermometry (75°–92°C) and the scarce fluid inclusion data (70°–140°C), this is the most suitable possibility to explain the sulfur isotope results at San Vicente. The alternative of introducing a brine with sulfur homogenized elsewhere in the basin does not explain the association of the ore with evaporite-bearing facies.

The range of oxygen and carbon isotope ratios in carbonates is very narrow. However, a clear trend to lighter isotope ratios in the late crystallization generations is recognized. This isotopic shift is regarded in terms of an evolving ore-forming fluid which changed its composition slowly but continuously during crystallization under conditions of burial diagenesis and steadily increasing temperature. The composition of this fluid is mainly determined by the mixing ratios with the host rock as well as by the introduction of a basinal brine. Subordinate incorporation of light organic carbon is possible. In situ meteoric influence can be ruled out since sharper changes would be expected.

It can be concluded that the San Vicente lead-zinc deposit formed during late stages of diagenesis under considerable burial by the introduction of a zinc- and lead-bearing basinal brine characterized by strontium isotope ratios slightly higher than contemporaneous seawater and highly radiogenic lead isotope ratios. The temperatures indicated by sulfur isotope geo-

thermometry, and also supported by preliminary fluid inclusion data, would be consistent with temperatures attained through the normal geothermal gradient at a burial depth of about 2 to 3 km by the end of the Jurassic period. A burial depth of about 2 to 3 km would also be consistent with conditions required for oil generation. This process is necessary to explain the deposition of massive bitumen in generation III. The oil generation could either take place close to the ore deposit, because the host rocks are rich in dispersed organic matter (the Bituminous Silty Limestone has been identified as an oil source rock), or hydrocarbons could be introduced by a basinal brine.

The genetic model of San Vicente is envisaged essentially as a single-stage event characterized by a progressive ore fluid evolution. For discussion purposes, the existence of two fluids can be considered: a fluid at the site of the ore deposit, from which the ore and gangue minerals precipitate, and an influxing basinal brine. Whereas the composition of the basinal brine can be considered to be relatively constant or to change only slowly, the composition of the fluid at the depositional site changes locally depending on various factors. The element content of this fluid is determined by the steady contribution of the basinal brine, but it also changes due to different fluid/host-rock mixing ratios in different parts of the ore deposit. Other parameters also play an important role, as, for instance, precipitation of new minerals, reduction of SO^{-4} to S^{-}, and eventually, incorporation of in situ organic carbon. Oil generation near the deposition site is a further possibility which must be considered. In addition, the physicochemical parameters (such as T, eH, and pH) of the ore fluid control the precipitation and/or dissolution of minerals and, in part, their isotopic ratios.

The evolution of the fluid has been traced using petrographic and geochemical evidence, including isotopic determinations on samples from different paragenetic positions. The contributions to the ore matter from the basinal brine and from the host rock can be envisaged as follows:

1. During the process of ore formation the strontium isotopes became progressively more radiogenic. This was due essentially to higher brine/host-rock ratios in the last generations. In addition, the strontium of the basinal brine became increasingly more radiogenic during basin evolution due to progressive leaching of rubidium-bearing silicates.

2. The stable isotopes (C and O) precipitating from the fluid became progressively slightly lighter. This trend results from a combination of temperature effects, different mixing fluid/host ratios, and incorporation of organic carbon, even without considering the otherwise probable influence of the input of the basinal brine.

3. The sulfur appears to have been abiogenically reduced near the deposition site and incorporated directly to the ore-forming fluid. During crystallization the sulfur isotope composition changed toward slightly lighter $\delta^{34}S$ ratios.

4. Lead and by analogy zinc have been supplied almost entirely by the basinal brine. Slightly scattering values along a mixing line indicate contributions from at least two lead sources. The scattering of the lead isotope ratios argues for compositional changes in the basinal brine during ore formation.

5. The fluid became enriched in the last stages of crystallization in bitumen, as evidenced by deposition of massive bitumen in generation III (always postdating the ore minerals). Both oil generation near the ore deposit and introduction of bitumen with the basinal brine can be considered.

6. The fluid probably also became richer in Sr, Rb, and Na because the late crystallization generations are relatively enriched in these elements.

Petrographic observations, in particular the almost total absence of repetitions in the paragenetic sequence, support the hypothesis of a single ore-forming event. This created manifold crystallization features, including diagenetic crystallization rhythmites and hydraulic breccias produced in an overpressure regime. Dolomite dissolution features, observed in breccias and in other structures, are probably due to the local abundance of hydrogen ions liberated by the replacement of sulfate by carbonate.

Textural and isotopic evidence indicates unequivocally that the gangue of coarsely crystalline dolomite and the ore minerals essentially formed during the same process. However, this dolomite may have been produced, at least in part, by recrystallization of a former dolomite that originated during early stages of diagenesis. This is strongly suggested by the strict facies-bound character of the dolomitic units. The lower strontium contents and the favorable depositional environment would be consistent with the existence of a former dolomite produced during early diagenesis.

Finally, some constraints can be placed regarding the time parameters and dynamics of the migration of the lead- and zinc-bearing brine that produced the San Vicente ore deposit. If the temperature range of 70° to 100°C is confirmed, an Upper Jurassic age could be envisaged, i.e., coeval with the burial of about 2 to 3 km due to sedimentation of the Lower Sarayaquillo Formation. The subsequent deposition during the Cretaceous of thick clastic sequences would result in higher temperatures (in the range of up to 200°C for a burial depth of 5,000 m). The only very slight radiogenic character of the strontium isotope ratios could indicate a relatively immature stage of the basin, although other reasons could also explain

this feature. The epeirogenic movements that uplifted the Marañón geoanticline, which dissected the Pucará basin at the end of the Jurassic, could have influenced the brine dynamics.

Acknowledgments

We express our appreciation to the staff of San Ignacio de Morococha, S. A., in San Vicente, especially to R. Tejada, Juan Neyra, and Juan Carlos Alcalde for their support during the present investigation. In addition to the individuals and institutions mentioned in the isotopic chapters we would like to thank E. Schroll, in Vienna, and in P. Soler, in Paris, for their permission to use unpublished analytical data. The present investigation has benefited by grants from the European Communities (contract MSM-010-D). We also acknowledge data from the unpublished Master's thesis of E. González and illustration drafting by E. Gonzalez, H. Schönfelder, and S. Rosas, Heidelberg. The manuscript has greatly benefited from valuable comments by Duncan Large and two *Economic Geology* reviewers.

REFERENCES

Allan, J. R., and Matthews, R. K., 1982, Isotope signature associated with early meteoric diagenesis: Sedimentology, v. 29, p. 797–817.

Amstutz, G. C., 1956, María Esperanza mine—San Ramón: La Aroya, Peru, Cerro de Pasco Corp., int. rept., 2 p.

Amstutz, G. C., and Park, W. C., 1971, The paragenetic position of sulfides in the diagenetic crystallization sequence: Soc. Mining Geologists Japan Spec. Issue 3, p. 280–282.

Anderson, G. M., 1983, Some geochemical aspects of sulfide precipitation in carbonate rocks, *in* Kisvarsanyi, G., Grant, S. K., Pratt, W. P., and Koenig, J. W., eds., International conference on Mississippi Valley type lead-zinc deposits. Proc. Vol.: Rolla, Univ. Missouri-Rolla Press, p. 61–76.

Anderson, G. M., and Garven, G., 1987, Sulfate-sulfide-carbonate associations in Mississippi Valley-type lead-zinc deposits: ECON. GEOL., v. 82, p. 482–488.

Audebaud, E., Capdevila, R., Dalmayrac, B., Debelmas, J., Laubacher, G., Levevre, C., Marocco, R., Martinez, C., Mattauer, M., Megard, F., Paredes, J., and Tomasi, P., 1973, Les traits geólogiques essentiels des Andes Centrales (Perou-Bolivie): Rev. Géog. Phys. Géologie Dynamique, v. 15, p. 73–113.

Banner, J. L., Hanson, G. N., and Meyers, W. J., 1988, Determination of initial Sr isotopic compositions of dolostones from the Burlington-Keokuk Formation (Mississippian): Constraints from cathodoluminiscence, glauconite paragenesis and analytical methods: Jour. Sed. Petrology, v. 58, p. 673–687.

Barnes, H. L., 1983, Ore-depositing reactions in Mississippi Valley-type deposits, *in* Kisvarsanyi, G., Grant, S. K., Pratt, W. P., and Koenig, J. W., eds., International conference on Mississippi Valley type lead-zinc deposits. Proc.: Rolla, Univ. Missouri-Rolla Press, p. 77–85.

Beales, F. W., 1967, Precipitation of lead-zinc ores in carbonate reservoirs as illustrated by Pine Point ore field, Canada: Inst. Mining Metallurgy Trans., v. 75, sec. B, p. B278–B285.

Bencini, A., and Turi, A., 1974, Mn distribution in the Mesozoic carbonate rocks from Lima Valley, northern Apennines: Jour. Sed. Petrology, v. 44, p. 774–782.

Burke, W. H., Denison, R. E., Hetherington, E. A., Koepnick, R. B., Nelson, H. F., and Otto, J. B., 1982, Variations of seawater $^{87}Sr/^{86}Sr$ throughout Phanerozoic time: Geology, v. 10, p. 516–519.

Capdevila, R., Mégard, F., Paredes, J., and Vidal, P., 1977, Le batholite de San Ramón, Cordillére Orientale du Pérou central: Geol. Rundschau, v. 66, p. 434–446.

Chaudhuri, S., 1978, Strontium isotopic composition of several oilfield brines from Kansas and Colorado: Geochim. et Cosmochim. Acta, v. 42, p. 329–331.

Chaudhuri, S., Broedel, V., and Clauer, N., 1987, Strontium isotopic evolution of oil-field waters from carbonate reservoir rocks in Bindley field, central Kansas, U.S.A.: Geochim. et Cosmochim. Acta, v. 51, p. 45–53.

Clauer, N., 1976, Géochemie isotopique du strontium des milieux sédimentaires. Application à la géochronologie de la couverture du craton ouest-africain: Sci. Geol., Paris, Mem. 45, 256 p.

Claypool, G. E., Holser, W. T., Kaplan, I. R., Sakai, H., and Zak, I., 1980, The age curves of sulfur and oxygen isotopes in marine sulfate and their mutual interpretations: Chem. Geology, v. 28, p. 199–260.

Craig, H., 1957, Isotopic standards for carbon and oxygen and correction factors for mass spectrometric analysis of carbon dioxide: Geochim. et Cosmochim. Acta, v. 12, p. 133–149.

Crocetti, C. A., Holland, H. D., and McKenna, L. W., 1988, Isotopic composition of lead in galenas from the Viburnum Trend, Missouri: ECON. GEOL., v. 83, p. 355–376.

Dalheimer, M., 1990, The Zn-Pb-Ag deposits Huaripampa and Carahuacra in the mining district of San Cristobal, central Peru, *in* Fontboté, L., Amstutz, G. C., Cardozo, M., Cedillo, E., and Frutos, J., eds., Stratabound ore deposits in the Andes: Berlin-Heidelberg-New York, Springer-Verlag, p. 279–291.

Delgado, F., 1977, Primary textures in dolostones and recrystallized limestones: A technique for their microscopic study: Jour. Sed. Petrology, v. 47, p. 1339–1341.

Dickson, J. A. D., and Coleman, M. L., 1980, Changes in carbon and oxygen isotope composition during limestone diagenesis: Sedimentology, v. 27, p. 107–118.

Doe, B. R., and Zartmann, R. E., 1979, Plumbotectonics: The Phanerozoic, *in* Barnes, H. L., ed., Geochemistry of hydrothermal ore deposits: New York, Wiley Intersci., p. 22–70.

Dunham, R. J., 1962, Classification of carbonate rocks according to depositional texture: Am. Assoc. Petroleum Geologists Mem. 1, p. 108–121.

Dunin, E., 1975, Control litológico y estratigráfico en la ubicación de los mantos con sulfuros de metales no ferrosos en las capas calcáreas del Perú central: Soc. Geol. Perú Bol., v. 50, p. 25–52.

Field, C. W., Rye, R. O., Dymond, J. R., Whelan, J. F., and Senechal, R. G., 1983, Metaliferous sediments of the East Pacific Rise, *in* Shanks, W. C., III, ed., Cameron volume of unconventional mineral deposits: New York, Soc. Mining Engineers, p. 133–156.

Flint, S., 1986, Sedimentary and diagenetic controls on red-bed ore genesis: The middle Tertiary San Bartolo copper deposit, Antofagasta province, Chile: ECON. GEOL., v. 81, p. 761–778.

Flint, S., Clemmey, H., and Turner, P., 1986, Conglomerate-hosted copper mineralization in Cretaceous Andean molasse: The Coloso Formation of northern Chile: Geol. Mag., v. 123, p. 525–536.

Fontboté, L., 1981, Strata-bound Zn-Pb-F-Ba deposits in carbonate rocks: New aspects of paleogeographic location, facies factors and diagenetic evolution. (With a comparison of occurrences from the Triassic of southern Spain, the Triassic/Liassic of central Peru and other localities): Unpub. Ph.D. dissert., Univ. Heidelberg, 193 p.

—— 1990, Stratabound ore deposits in the Pucará Group—an overview, *in* Fontboté, L., Amstutz, G. C., Cardozo, M., Cedillo, E., and Frutos, J., eds., Stratabound ore deposits in the Andes: Berlin-Heidelberg-New York, Springer-Verlag, p. 253–266.

Fontboté, L., and Amstutz, G. C., 1983, Facies and sequence analysis of diagenetic crystallization rhythmites in strata-bound Pb-Zn-(Ba-F) deposits in the Triassic of central and southern

Europe, *in* Schneider, H. G., ed., Mineral deposits of the Alps and of the Alpine epoch in Europe: Heidelberg, Springer-Verlag, p. 347–358.

Fontboté, L., and Gorzawski, H., 1987, Petrographic and geochemical indicators for the exploration of hidden ore deposits in sedimentary rocks: Brussels, Comm. European Communities, unpub. final rept. contract MSM-010-D, 221 p.

—— 1988, Isotope (Sr, C, O, S) tracing of diagenetic ore formation in carbonate-hosted deposits illustrated on the F-(Pb-Zn) deposits in the Alpujarrides, Spain and the San Vicente Zn-Pb Mine, Perú: Soc. Geology Appl. Mineral Deposits Spec. Pub. 6, p. 465–484.

Fontboté, L., Amstutz, G. C., and Samaniego, A., 1981, Zur faziellen Stellung und zum diagenetischen Kristallisationsprozess von Erzmineralien in schichtgebundenen Zn-Pb-Lagerstätten (am Beispiel von San Vicente, im zentralen Ostperu). Proc. Geowiss. Lateinamerika Koll., 7th, Heidelberg, 1980: Zentralbl. Geologie Paläontologie, Jg. 1981, Teil I, p. 465–477.

Fontboté, L., Calvez, J. Y., Pincheira, M., and Wolf, F., 1990a, Geotectonic position and metal sources of stratabound ores in the central Andes—lead isotopic constraints: ORSTOM Internat. Symposium Andean Geodynamics, Grenoble, May 15–17, 1990, Collection Colloques et Seminaires, p. 347–350.

Fontboté, L., Gunnesch, K. A., and Baumann, A., 1990b, Metal sources in stratabound ore deposits in the Andes (Andean cycle): Lead isotopic constraints, *in* Fontboté, L., Amstutz, G. C., Cardozo, M., Cedillo, E., and Frutos, J., eds., Stratabound ore deposits in the Andes: Berlin-Heidelberg-New York, Springer-Verlag, p. 759–773.

Gieskes, G. M., Elderfield, H., and Palmer, M. R., 1986, Strontium and its isotopic composition in interstitial waters of marine carbonate sediments: Earth Planet. Sci. Letters, v. 77, p. 229–235.

González, E., 1987, Petrographische und geochemische Untersuchungen an die Sedimentabfolge des Pucaras in der schichtgebundenen Zn-Pn Lagerstätte San Vicente, Perú: Unpub. Diplomarbeit, Univ. Heidelberg, 128 p.

González, E., and Fontboté, L., 1986, Petrographic and lithogeochemical investigations on the Pucará Group in the carbonate-hosted Zn-Pb deposit of San Vicente, Perú [abs.]: Berliner Geowiss. Abh., Reihe A, Sonderband, p. 126–127.

Gorzawski, H., Fontboté, L., Sureau, A., and Calvez, J. Y., 1989, Strontium isotope trends during diagenesis in ore-bearing carbonate basins: Geol. Rundschau, v. 78, p. 269–290.

Gorzawski, H., Fontboté, L., Field, C. W., and Tejada, R., 1990, Sulfur isotope studies in the zinc-lead mine San Vicente, central Peru, *in* Fontboté, L., Amstutz, G. C., Cardozo, M., Cedillo, E., and Frutos, J., eds., Stratabound ore deposits in the Andes: Berlin-Heidelberg-New York, Springer-Verlag, p. 305–312.

Grant, N. K., and Miranda, C. B., 1983, Strontium isotope and rare earth element variations in non-sulphide minerals from the Elmwood-Gordonsville mines, central Tennessee, *in* Kisvarsanyi, G., Grant, S. K., Pratt, W. P., and Koenig, J. W., eds., International conference on Mississippi Valley type lead-zinc deposits. Proc. Vol.: Rolla, Univ. Missouri-Rolla Press, p. 206–210.

Gunnesch, K. A., Baumann, A., and Gunnesch, M., 1990, Lead isotope variations across the central Peruvian Andes: ECON. GEOL., v. 85, p. 1384–1401.

Hagni, R. D., 1983, Ore microscopy, paragenetic sequence, trace element content, and fluid inclusion studies of the copper-lead-zinc deposits in the southeast Missouri lead district, *in* Kisvarsanyi, G., Grant, S. K., Pratt, W. P., and Koenig, J. W., eds., International conference on Mississippi Valley type lead-zinc deposits. Proc. Vol.: Rolla, Univ. Missouri-Rolla Press, p. 243–256.

Hannah, J. L., and Stein, H. J., 1984, Evidence for changing ore fluid composition: Stable isotope analyses of secondary carbonates, Bonneterre Formation, Missouri: ECON. GEOL., v. 79, p. 1930–1935.

Heyl, A. V., Landis, G. P., and Zartman, R. E., 1974, Isotopic evidence for the origen of Mississippi Valley-type mineral deposits: ECON. GEOL., v. 69, p. 992–1006.

Irwin, H., Curtis, C., and Coleman, M., 1977, Isotopic evidences for source of diagenetic carbonates formed during burial of organic-rich sediments: Nature, v. 269, p. 209–213.

Japan International Cooperation Agency, 1976, Report on geological survey of the Cordillera Oriental, central Peru: Lima, Japan Mining Agency, Japan Internat. Coop. Agency, unpub. rept., v. 2, p. 39–40.

—— 1979, Report on geological survey of the Cordillera Oriental, central Peru: Lima, Japan Mining Agency, Japan Internat. Coop. Agency, unpub. rept., v. 8, 46 p.

Kelts, K., and McKenzie, J. A., 1982, Diagenetic dolomite formation in Quaternary anoxic diatomaceous muds of Deep Sea Drilling Project Leg 64, Gulf of California, *in* Deep Sea Drilling Proj., Initial Repts., v. 64, p. 553–569.

Kesler, S. E., Jones, L. M., and Ruiz, J., 1988, Strontium isotopic geochemistry of Mississippi Valley-type deposits, east Tennessee: Implications for age and source of mineralizing brines: Geol. Soc. America Bull., v. 100, p. 1300–1307.

Kessen, K., Woodruff, M. S., and Grant, N. K., 1981, Gangue mineral $^{87}Sr/^{86}Sr$ ratios and the origin of Mississippi Valley mineralizations: ECON. GEOL., v. 76, p. 913–920.

Kobe, H. W., 1977, El Grupo Pucará y su mineralización en el Perú central: Soc. Geol. Perú Bol., v. 55–56, p. 61–84.

—— 1982, El ambiente de la mineralización estratoligada de Zn-Pb-Ag-Ba-Mn-Fe-Cu en los sedimentos de la cuenca occidental del Pucará, Perú central: Soc. Geol. Perú Bol., v. 69, p. 41–69.

Kontak, D. J., Clark, A. H., Farrar, E., and Strong, D. F., 1985, The rift associated Permo-Triassic magmatism of the Eastern Cordillera: A precursor of the Andean orogeny, *in* Pitcher, W. S., Atherton, M. P., Cobbing, E. J., and Beckinsale, R. D., eds., Magmatism at a plate edge: The Peruvian Andes: Glasgow, Blackie and Son, Ltd., p. 36–44.

Lancelot, J. R., Laubacher, G., Marocco, R., and Renaud, U., 1978, U/Pb radiogeochronology of two granitic plutons from the Eastern Cordillera (Perú)—extent of Permian magmatic activity and consequences: Geol. Rundschau, v. 67, p. 236–243.

Land, L. S., 1983, The application of stable isotopes to studies of the origin of dolomite and to problems of diagenesis of clastic sediments: Soc. Econ. Paleontologists Mineralogists, v. 10, p. 4-1–4-22.

Lange, S., Chaudhuri, S., and Clauer, N., 1983, Strontium isotopic evidence for the origin of barites and sulfides from the Mississippi Valley-type ore deposits in southeast Missouri: ECON. GEOL., v. 78, p. 1255–1261.

Lavado, M., 1980, Geologic aspects of the ore occurrences at the San Vicente mine, San Ramon, Central Perú: Unpub. M.Sc. thesis, Dallas, Univ. Texas, 127 p.

Levin, P., 1974, Die Pucara-Sedimente in Chanchamayo-Gebiet in Ost-Perú: Geol. Rundschau, v. 63, p. 345–356.

—— 1975, Der petrographisch-geologische Rahmen des Chanchamayo-Gebietes in Ost- Peru und die Deutung seiner schichtgebundeneen Vererzungen. Entwurf einer Metallogenese der östlichen Zentral-Perú: Unpub. Ph.D. dissert., Univ. Heidelberg, 242 p.

Levin, P., and Amstutz, G. C., 1973, Neue Untersuchungen über schichtgebundene Lagerstätten im zentralen Ostperu: Münstersche Forschungen Geologie Paläontologie, v. 31/32, p. 233–259.

Loughman, D. L., and Hallam, A., 1982, A facies analysis of the Pucará Group (Norian to Toarcian carbonates, organic-rich shale and phosphate) of central and northern Perú: Sed. Geology, v. 32, p. 161–194.

Macfarlane, A. W., 1989, Lead, sulfur and strontium isotopes in the Hualgayoc area, Perú, and lead isotope provinces of the central Andes: Unpub. Ph.D. thesis, Cambridge, Harvard Univ., 370 p.

MacQueen, R. W., and Powell, T. G., 1983, Organic geochemistry of the Pine Point lead-zinc ore field and region, northwestern Territories, Canada: ECON. GEOL., v. 78, p. 1–25.

McCrea, J. M., 1950, On the isotopic chemistry of carbonates and a paleotemperature scale: Jour. Chem. Physics, v. 18, p. 849–857.

Medford, G. A., Maxwell, R. J., and Armstrong, R. L., 1983, $^{87}Sr/^{86}Sr$ ratio measurements on sulfides, carbonates, and fluid inclusions from Pine Point, Northwest Territories, Canada: An $^{87}Sr/^{86}Sr$ ratio increase accompanying the mineralization process: ECON. GEOL., v. 78, p. 1375–1378.

Mégard, F., 1968, Geología del Cuadrángulo de Huancayo: Servicio Geol. Minero Bol., v. 18, 123 p.

—— 1978, Etude géologique des Andes du Perou central: ORSTOM Mem., v. 86, 303 p.

—— 1984, The Andean orogenic period and its major structures in central and northern Perú: Geol. Soc. London Jour., v. 14, p. 893–900.

Meyers, W. J., and Lohmann K. C., 1985, Isotope geochemistry of regionally extensive calcite cement zones and marine components in Mississippian limestones, New Mexico: Soc. Econ. Paleontologists Mineralogists Spec. Pub. 36, p. 223–239.

Moore, C. H., 1985, Upper Jurassic subsurface cements: A case history: Soc. Econ. Paleontologists Mineralogists Spec. Pub. 36, p. 291–308.

Mukasa, S., 1984, Comparative Pb isotope systematics and zircon U-Pb geochronology for the Coastal, San Nicolas and Cordillera Blanca batholiths, Perú: Unpub. Ph.D. thesis, Santa Barbara, Univ. California, 383 p.

Ohmoto, H., and Rye, R. O., 1979, Isotopes of sulfur and carbon, *in* Barnes, H. L., ed., Geochemistry of hydrothermal ore deposits: New York, Wiley Intersci., p. 509–567.

Orr, W. L., 1974, Changes in sulfur content and isotopic ratios of sulfur during petroleum maturation—study of Big Horn basin Paleozoic oils: Am. Assoc. Petroleum Geologists Bull., v. 58, p. 2295–2318.

—— 1977, Geological and geochemical controls on the distribution of hydrogen sulfide in natural gas, *in* Campos, R., and Goni, J., eds., Advances in organic geochemistry: Madrid, Empresa Nacional Adaro Investigaciones Mineras, Sociedad Anónima, p. 571–597.

Palacios, O., 1980, El Grupo Pucará en la región Subandina (Perú central): Soc. Geol. Perú Bol., v. 67, p. 153–162.

Pardo, A., 1983, A facies analysis of the Pucará Group (Norian to Toarcian carbonates, organic-rich shale and phosphate) of central and northern Perú—comment: Sed. Geology, v. 35, p. 215–223.

Pardo, A., and Sanz, V., 1979, Estratigrafía del curso medio del Río La Leche, Departamento de Lambayeque: Soc. Geol. Perú Bol., v. 67, p. 153–162.

Powell, T. G., and MacQueen, R. W., 1984, Precipitation of ores and organic matter: Sulfate reactions at Pine Point, Canada: Science, v. 224, p. 63–66.

Prinz, P., 1985a, Stratigraphie und Ammonitenfauna der Pucará-Gruppe (Obertrias- Unterjura) von Nord-Perú: Stuttgart, Paleontographica, Abt. A., v. 188, p. 153–197.

—— 1985b, Zur Stratigraphie und Ammonitenfauna der Pucará-Gruppe bei San Vicente: Dept. Junin, Perú: Stuttgart-Berlin, Newsl. Stratigr., v. 14, p. 129–141.

Puig, A., 1988, The geologic and metallogenetic significance of lead isotope composition of lead in galena of the Chilean Andes: ECON. GEOL., v. 83, p. 843–858.

Rickard, D., 1983, Precipitation and mixing mechanisms in Laisvall-type sandstone lead-zinc deposits *in* Kisvarsanyi, G., Grant, S. K., Pratt, W. P., and Koenig, J. W., eds., International conference on Mississippi Valley type lead-zinc deposits. Proc. Vol.: Rolla, Univ. Missouri-Rolla Press, p. 449–458.

Russell, C. W., 1985, A strontium isotope study of oil field brines and associated rocks in southeastern Mississippi: Unpub. M.S. thesis, Florida State Univ., 176 p.

Schulz, G. G., 1971, Die schichtgebundene Zinkblende Lagerstätte San Vicente in Ost-Perú und ihr geologischer Rahmen: Unpub. Ph.D. dissert., Univ. Aachen, 165 p.

Sharma, T., and Clayton, R. N., 1965, Measurement of $^{18}O/^{16}O$ ratios of total oxygen of carbonates: Geochim. et Cosmochim. Acta, v. 29, p. 1347–1353.

Soler, P., 1987, Variations des teneurs en elements mineurs (Cd, In, Ge, Ga, Ag, Bi, Se, Hg, Sn) des minerais de Pb-Zn de la province polymétallique des Andes du Pérou central: Mineralium Deposita, v. 22, p. 135–143.

Spirakis, C. S., 1986, The valence of sulfur in disulfides—an overlooked clue to the genesis of Mississippi Valley-type lead-zinc deposits: ECON. GEOL., v. 81, p. 1544–1545.

Starinski, A., Bielski, M., Lazar, B., Steinitz, G., and Raab, M., 1983, Strontium isotopic evidence on the history of oilfield brines, Mediterranean Coastal plain, Israel: Geochim. et Cosmochim. Acta, v. 47, p. 687–695.

Stueber, A. M., Pushkar, P., and Hetherington, E. A., 1984, A strontium isotopic study of Smackover brines and associated solids, southern Arkansas: Geochim. et Cosmochim. Acta, v. 48, p. 1637–1649.

Sunwall, M. T., and Pushkar, P., 1979, The isotopic composition of strontium in brines from petroleum fields of southeastern Ohio: Chem. Geology, v. 24, p. 189–197.

—— 1984, Oil field brines as ore-forming solutions: ECON. GEOL., v. 79, p. 23–37.

Szekely, T. S., and Grose, L. T., 1972, Stratigraphy of the carbonate black shale and phosphate of the Pucará Group (Upper Triassic-Lower Jurassic), central Andes, Perú: Geol. Soc. America Bull., v. 83, p. 407–428.

Tayler, J. R., 1962, Exploration Uchubamba area, Jauja, Junin: New York, Eastern Andes Corporation, June Rept., 2 p. (unpub. rept.).

Trudinger, P. A., Chambers, L. A., and Smith, J. W., 1985, Low temperature sulphate reduction: Biological vs. abiological: Canadian Jour. Earth Sci., v. 12, p. 1910–1918.

Veizer, J., and Compston, W., 1974, $^{87}Sr/^{86}Sr$ composition of seawater during the Panerozoic: Geochim. et Cosmochim. Acta, v. 38, p. 1461–1484.

Veizer, J., and Hoefs, J., 1976, The nature of O^{18}/O^{16} and C^{13}/C^{12} secular trends in sedimentary carbonate rocks. Geochim. et Cosmochim. Acta, v. 40, p. 1387–1395.

Walter, L. M., Brannon, J. C., Moldovany, E. P., and Podosek, F. A., 1987, Sr and S isotopic data on diagenetic sulfides, sulfates and calcites (Smackover Fm., S. W. Arkansas): Implications for fluid sources and chemical evolution [abs.]: Soc. Econ. Paleontologists Mineralogists Ann. Midyear Mtg., Austin, Texas, 1987, v. 4, p. 88.

Wedepohl, K. H., 1974, Handbook of geochemistry: Berlin, Springer-Verlag, v. 11-4, p. 38K-1–38K-13.

Woronick, R. E., and Land, L. S., 1985, Late burial diagenesis, Lower Cretaceous Pearsall and Lower Glen Rose Formations, south Texas: Soc. Econ. Paleontologists Mineralogists Spec. Pub. 36, p. 265–275.